



# รายงานวิจัยฉบับสมบูรณ์

# การกำจัดคลื่นที่ถูกตรึงด้วยสิ่งกีดขวางรูปร่างและการเรียงตัวต่างกัน ในตัวกลางเคมีกระตุ้นได้

โดย

ผศ. ดร. ชัยยะ เหลืองวิริยะ และ คณะ

# รายงานวิจัยฉบับสมบูรณ์

# การกำจัดคลื่นที่ถูกตรึงด้วยสิ่งกีดขวางรูปร่างและการเรียงตัวต่างกัน ในตัวกลางเคมีกระตุ้นได้

ผศ. ดร. ชัยยะ เหลืองวิริยะ	มหาวิทยาลัยเกษตรศาสตร์	(หัวหน้าโครงการ)
ผศ. มาลี สุทธิโอภาส	มหาวิทยาลัยเกษตรศาสตร์	(ผู้ร่วมวิจัย)
ผศ. ดร. จริน กาญจนวริน	มหาวิทยาลัยเกษตรศาสตร์	(ผู้ร่วมวิจัย)
ผศ. ดร. จิราพร เหลืองวิริยะ	มหาวิทยาลัยพระจอมเกล้าพระนครเหร	นื้อ (ผู้ร่วมวิจัย)
ผศ. ดร. บุษยรัตน์ ธรรมพัฒนกิจ	จุฬาลงกรณ์มหาวิทยาลัย	(หักวิจัยที่ปรึกษา)

สนับสนุนโดยสำนักงานคณะกรรมการการอุดมศึกษา สำนักงานกองทุนสนับสนุนการวิจัย และ มหาวิทยาลัยเกษตรศาสตร์ (ความเห็นในรายงานนี้เป็นของผู้วิจัย สกอ. และ สกว. ไม่จำเป็นต้องเห็นด้วยเสมอไป)

### บทคัดย่อ

รหัสโครงการ: TRG5680044

ชื่อโครงการ: การกำจัดคลื่นที่ถูกตรึงด้วยสิ่งกีดขวางรูปร่างและการเรียงตัวต่างกันในตัวกลางเคมีกระตุ้นได้

**ชื่อนักวิจัย :** ผศ. ดร. ชัยยะ เหลืองวิริยะ มหาวิทยาลัยเกษตรศาสตร์

อีเมลส์: fscicyl@ku.ac.th ระยะเวลาโครงการ: 2 ปี

บทคัดย่อ:

คลื่นสไปรอลในตัวกลางกระตุ้นได้ซึ่งเกิดขึ้นในตัวกลางชนิดต่างๆ กัน สามารถอธิบายได้ด้วยกลไก ปฏิกิริยาและการแพร่ที่คล้ายคลึงกัน คลื่นประเภทนี้มีผลกระทบต่อสุขภาพของมนุษย์ กล่าวคือ คลื่น ศักย์ไฟฟ้าในรูปแบบสไปรอลเป็นสาเหตุของโรคหัวใจบางชนิด เช่น ventricular tachycardia และ ventricular fibrillation อันเป็นสาเหตุหลักของหัวใจวาย ในส่วนของงานวิจัยด้านการทดลองนิยมใช้ตัวกลาง เคมีปฏิกิริยาบิโลซอฟ-ซาบอทินสกี เนื่องด้วย ความสะดวกในการเตรียมตัวกลางตลอดจนการบันทึกผลการ ทดลอง โครงการวิจัยนี้มีวัตถุประสงค์เพื่อศึกษาอิทธิพลของรูปร่างและการเรียงตัวของสิ่งกีดขวางต่อการ เคลื่อนที่ของคลื่นสไปรอลและการกำจัดคลื่นที่ถูกตรึงดังกล่าวด้วยสนามไฟฟ้าในตัวกลางเคมี โดยผลการ ทดลองได้รับการยืนยันจากการจำลองแบบทางคอมพิวเตอร์

เมื่อความหนาแน่นกระแสไฟฟ้ามีค่ามากพอคือ  $J_{\rm unpin}$ , หัวสไปรอลซึ่งถูกตรึงด้วยสิ่งกีดขวางวงกลมจะ ถูกดึงออกและเลื่อนห่างออกจากสิ่งกีดขวาง โดยค่าวิกฤติ  $J_{\rm unpin}$  มีขนาดเพิ่มขึ้นตามขนาดเส้นผ่านศูนย์กลาง ของสิ่งกีดขวาง d อีกทั้งอัตราการเพิ่ม  $\Delta J_{\rm unpin}/\Delta d$  มีค่ามากสำหรับสิ่งกีดขวางที่มีขนาดใหญ่กว่าแกนของสไปรอล จากผลการทดลองด้านอิทธิพลของรูปร่างของสิ่งกีดขวางโดยใช้สิ่งกีดขวางวงกลมและสี่เหลี่ยมผืนผ้า พบว่า สไปรอลที่ถูกตรึงมีควายาวคลื่น คาบเวลาและความเร็วเพิ่มขึ้นตามเส้นรอบวงของสิ่งกีดขวางโดยไม่ ขึ้นกับพื้นที่ของสิ่งกีดขวาง รูปทรงของคลื่นสไปรอลขึ้นกับรูปร่างของสิ่งกีดขวาง คลื่นสไปรอลที่ถูกตรึงกับ วงกลมหรือสี่เหลียมจตุรัสมีรูปทรงใกล้เคียงกับสไปรอลอาร์คีมีเดียน แต่สำหรับกรณีสี่เหลียมผืนผ้าที่ยาว เรียว รูปทรงของคลื่นสไปรอลสามารถสร้างโดยการต่อครึ่งวงกลมที่มีขนาดสัมพันธ์กับความยาวของสิ่งกีด ขวาง

คำหลัก: ตัวกลางที่ถูกกระตุ้นได้, คลื่นสไปรอล, ปฏิกิริยาบิโลซอฟ-ซาบอทินสกี, กลไกปฏิกิริยาและการ แพร่, การตรึง

### **Abstract**

Project Code: TRG5680044

**Project Title:** Elimination of waves pinned to obstacles with different shapes and orientations in

excitable chemical media

**Investigator:** Assist. Prof. Dr. Chaiya Luenqviriya, Kasetsart University

E-mail Address: fscicyl@ku.ac.th

**Project Period**: 2 years

**Abstract:** 

Spiral waves evolving in various excitable media are governed by similar reaction-diffusion mechanisms. They also have an important impact on human health conditions. Spiral waves of electrical excitation in the heart and their instabilities are involved in causing certain types of cardiac arrhythmia, such as ventricular tachycardia and fibrillations, which can potentially lead to sudden cardiac death. The Belousov-Zhabotinsky (BZ) reaction is one of the most popular model systems to study the dynamics of spiral waves experimentally, because of both its easy preparation and the convenient detection of the wave patterns occurring in this reaction. Our research project aims to investigate the influence of the obstacle shape and orientation on the dynamics of a spiral wave and the elimination of such pinned spiral wave using an applied electric field in chemical BZ media. To confirm experimental results, computer simulations are also performed.

When the applied electric current density reaches the necessary current density  $J_{unpin}$ , the spiral tip, pinned to a circular obstacle, is detached and subsequently drifts away from the obstacle.  $J_{unpin}$  is found to increase with the obstacle diameter d. The growth rate  $\Delta J_{unpin}/\Delta d$  is much higher for obstacles larger than the free spiral core as compared to that for smaller obstacles. From our study of the influence of obstacle shape using circular and rectangular obstacles, the propagating parameters i.e. wavelength, wave period, and velocity of pinned spiral waves increase with the circumference, regardless of the obstacle area. Despite these common features of the parameters, the forms of pinned spiral waves depend on the obstacle shapes. The structures of spiral waves pinned to circles as well as squares are similar to Archimedean spirals. For extremely thin rectangles, the spiral form can be constructed by employing semicircles with different radii which relate to the obstacle width and the core diameter of free spirals.

**Keywords:** excitable media, spiral wave, Belousov-Zhabotinsky reaction, reaction-diffusion mechanism; pinning

# กิตติกรรมประกาศ

คณะผู้วิจัยขอขอบคุณ สำนักงานคณะกรรมการการอุดมศึกษา สำนักงานกองทุนสนับสนุนการวิจัย และ มหาวิทยาลัยเกษตรศาสตร์ สำหรับเงินทุนวิจัย ในโครงการนี้

ผศ. ดร. ชัยยะ เหลืองวิริยะ (หัวหน้าโครงการวิจัย)

# 1. บทนำ

# 1.1 ความสำคัญและที่มาของปัญหา

โครงการวิจัยนี้มีวัตถุประสงค์เพื่อศึกษาอิทธิพลของรูปร่างและการเรียงตัวของสิ่งกีดขวางต่อการ เคลื่อนที่ของคลื่นสไปรอลและการกำจัดคลื่นที่ถูกตรึงดังกล่าวด้วยสนามไฟฟ้าในตัวกลางเคมีปฏิกิริยาบิโล ซอฟ-ซาบอทินสกี พลศาสตร์ของคลื่นในตัวกลางที่ถูกกระตุ้นได้ (excitable media) ซึ่งมีความสำคัญดังเช่น คลื่นในตัวกลางสองมิติเกี่ยวข้องกับการกำจัดก๊าซมลพิษจากท่อไอเสีย (clean exhaust) [3] ซึ่งเป็นผลงาน ส่วนหนึ่งที่ทำให้ศาสตราจารย์แอรทล์ (Prof. G. Ertl) ได้รับรางวัลโนเบลสาขาเคมี ในปี ค.ศ. 2007 [4]

ในส่วนของคลื่นสามมิตินั้น นักวิทยาศาสตร์จากหลายแขนงสาขาให้ความสนใจอย่างมากเนื่องจากมี ผลการวิจัยโดยใช้เนื้อเยื่อหัวใจจากสัตว์ [17] ที่สนับสนุนว่า คลื่นศักย์ไฟฟ้าในสามมิติที่เรียกว่าคลื่นสกอล์ (scroll wave) เป็นสาเหตุของโรคหัวใจบางชนิด เช่น ventricular tachycardia ซึ่งมีผลให้จังหวะการเต้นของ หัวใจเร็วขึ้นแต่ประสิทธิภาพการสูบฉีดโลหิตลดลง การที่คลื่นดำรงอยู่ในหัวใจได้นานนั้นเชื่อว่าเกิดจากการที่ คลื่นถูกตรึงไว้กับจุดบกพร่อง (localized defect) ในตัวกลาง

สถานการณ์จะเลวร้ายมากขึ้นหากเกิดปรากฏการณ์คลื่นโกลาหลของวินฟรี (Winfree turbulence) [18] ซึ่งเรียกขานตามชื่อศาสตราจารย์วินฟรี (Prof. A.T. Winfree) ผู้รายงานการพบปรากฏการณ์ สิ่งที่ น่าสนใจคือ ปรากฏการณ์นี้เกิดเฉพาะในแผ่นเนื้อเยื่อหัวใจที่หนา (สามมิติ) เท่านั้น ปรากฏการณ์คลื่น โกลาหลนี้มีผลให้เกิดภาวะ ventricular fibrillation อันเป็นสาเหตุหลักของหัวใจวาย ผลกระทบโดยตรงต่อ มนุษย์นี้เป็นปัจจัยหนึ่งที่กระตุ้นให้เกิดการวิจัยในด้านการควบคุมพลศาสตร์ของคลื่นทั้งในสองและสามมิติ รวมทั้งการระงับความโกลาหลของคลื่น อย่างกว้างขวางในช่วงสองทศวรรษที่ผ่านมา [20]

เป็นที่ทราบกันดีว่า ในหัวข้อวิจัยเดียวกันนั้น การทดลองคลื่นในสามมิติซับซ้อนมากกว่าการทดลอง สองมิติ โครงการวิจัยนี้จึงศึกษาคลื่นในสองมิติเพื่อให้ได้เงื่อนไขทางการทดลองที่เหมาะสม ผลจาก โครงการวิจัยนี้จะเป็นเครื่องชี้นำให้กับการทดลองในสามมิติในโครงการวิจัยต่อๆไป ในโครงการนี้ได้เลือก ศึกษาคลื่นในตัวกลางเคมี คือ ปฏิกิริยาบิโลซอฟ-ซาบอทินสกี (Belosov-Zhabotinsky reaction) [6,7] โดย จะใช้ปฏิกิริยาที่ได้รับการปรับปรุงแล้วซึ่งมีส่วนผสมของไพโรแกลลอล (pyrogallol) [28-30] เพื่อหลีกเลี่ยง ปัญหาฟองอากาศซึ่งรบกวนการเคลื่อนที่ของคลื่นเมื่อทำการทดลองเป็นเวลานาน

การเลือกศึกษาตัวกลางแบบเคมีนั้นมีเหตุผลสองประการคือ ประการแรก เป็นที่ยอมรับในวงการ วิจัยว่า พลศาสตร์ของคลื่นในตัวกลางที่ถูกกระตุ้นได้ชนิดต่าง ๆกันนั้นเกิดจากกลไกเดียวกันคือ กลไก ปฏิกิริยาและการแพร่ (reaction-diffusion mechanism) [1] ซึ่งตัวกลางแต่ละชนิดอาจมีรายละเอียดที่ต่างกัน ดังนั้นความรู้ที่ได้จากการศึกษาคลื่นในตัวกลางเคมีจึงสามารถนำไปประยุกต์ใช้กับตัวกลางอื่นๆได้ และ ประการที่สอง การเตรียมตัวกลางเคมีง่ายกว่าตัวกลางแบบสิ่งมีชีวิตและย่อมทำการทดลองซ้ำเพื่อยืนยั ผลได้ง่ายกว่า

# 1.2 วัตถุประสงค์ของโครงการวิจัย

- 1. เพื่อศึกษาอิทธิพลของรูปร่างและการเรียงตัวของสิ่งกีดขวางต่อการเคลื่อนที่ของคลื่นสไปรอลใน ตัวกลางเคมีปฏิกิริยาบิโลซอฟ-ซาบอทินสกี
- 2. เพื่อศึกษาการกำจัดคลื่นสไปรอลที่ถูกตรึงด้วยสนามไฟฟ้าในตัวกลางเคมีปฏิกิริยาบิโลซอฟ-ซาบอ ทินสกี

## 1.3 ประโยชน์ที่คาดว่าจะได้รับ

ผลจากโครงการวิจัยนี้จะทำให้พลศาสตร์ของคลื่นทั้งในสองมิติกระจ่างมากขึ้นและคาดว่าจะได้ผลงานตาม วัตถุประสงค์ที่ตั้งไว้ เพื่อเพื่อเผยแพร่ในวารสารวิชาการนานาชาติ

### 1.4 ขอบเขตของโครงการวิจัย

โครงการวิจัยนี้มุ่งเน้นศึกษาตัวกลางเคมีซึ่งมีความเข้มข้นของสารตั้นต้นในช่วงต่ำซึ่งทำให้คลื่ สไปรอลในตัวกลางนี้มีอัตราเร็วไม่มากนัก และกระแสไฟฟ้าที่ใช้ป้อนเพื่อบังคับคลื่นสไปรอลมีค่าต่ำเพื่อหลี เลี่ยงการเกิดความร้อนปริมาณมากในตัวกลางเคมี

# 2. ทฤษฎี

# ตัวกลางที่ถูกกระตุ้นได้และคลื่นสไปรอล

ปรากฏการณ์คลื่นในตัวกลางที่ถูกกระตุ้นได้ (excitable media) เกิดขึ้นในตัวกลางชนิดต่าง ๆกัน แต่ สามารถอธิบายได้ด้วยทฤษฎีเดียวกัน คือ กลไกปฏิกิริยาและการแพร่ (reaction-diffusion mechanism) [1] ของตัวกระตุ้น (activator) ซึ่งทำหน้าที่นำคลื่น และ ตัวยับยั้ง (inhibitor) ซึ่งทำหน้าที่ลดบทบาทของ ตัวกระตุ้น กลไกปฏิกิริยาและการแพร่นี้ทำให้คลื่นในตัวกลางที่ถูกกระตุ้นได้มีลักษณะเฉพาะตัว กล่าวคือ ใน ตัวกลางที่บางมาก (สองมิติ) หากหน้าคลื่นถูกทำให้ขาดเกิดเป็นปลายเปิด ปลายเปิดนั้นจะขดมัวนเกิดเป็น คลื่นสไปรอล (spiral wave) [2] และจะเกิดคลื่นในตัวกลางอย่างไม่มีที่สิ้นสุดโดยไม่ต้องการแหล่งกำเนิด คลื่นจากภายนอก ในกรณีนี้จุดที่ปลายเปิดหรือหัวสไปรอล (spiral tip) ทำหน้าที่เสมือนแหล่งกำเนิดคลื่น และมักเรียกว่าศูนย์บัญชาการ (organizing center) ของคลื่น

ตัวอย่างคลื่นสไปรอลในตัวกลางต่างๆ (รูปที่ 2.1 ก-ค) ได้แก่ คลื่นออกซิเดชันของคาร์บอนมอนอก ไซด์บนผิวทองคำขาว (clean exhaust) [3,4] คลื่นการรวมตัวกันของราเมือก [5] รวมทั้งคลื่นความเข้มข้น (concentration wave) ในตัวกลางปฏิกิริยาบิโลซอฟ-ซาบอทินสกี (Belosov-Zhabotinsky reaction) [6,7] ซึ่งเป็นที่นิยมใช้ในการวิจัยมากกว่าตัวกลางอื่นๆในสาขานี้ งานวิจัยคลื่นสไปรอลในตัวกลางปฏิกิริยานี้พบว่า วิถีหัวสไปรอล (spiral tip trajectory) อาจเป็นรูปแบบอย่างง่ายคือวงกลม หรือ รูปแบบที่ซับซ้อนซึ่งเรียกว่า

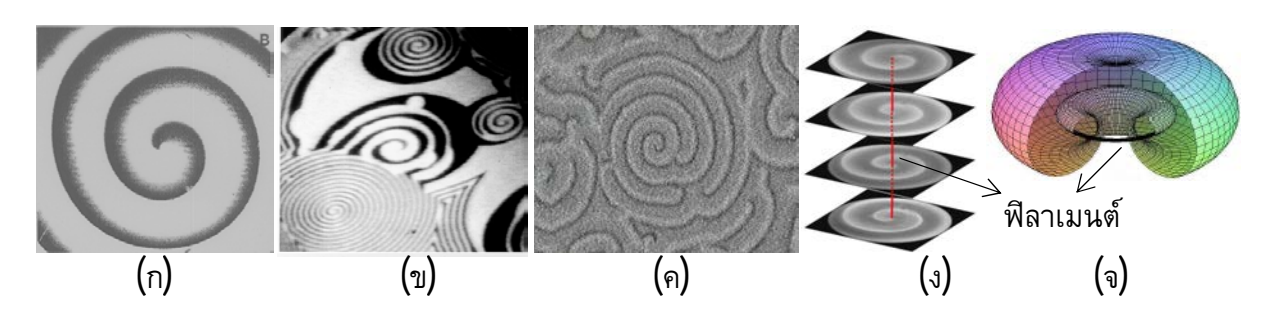
มีอันเดอริ่ง (meandering) [8-10] อีกทั้งวิถีหัวสไปรอลสามารถควบคุมได้โดยปัจจัยภายนอก เช่น แสง [11,12] หรือ สนามไฟฟ้า [13,14]

## คลื่นสกอล์และโรคหัวใจบางชนิด

สำหรับคลื่นในตัวกลางสามมิติเรียกว่าคลื่นสกอล์ (scroll wave) [15] สามารถเทียบเคียงได้กับการ นำตัวกลางสองมิติที่มีคลื่นสไปรอลมาซ้อนต่อกัน ในกรณีนี้ศูนย์บัญชาการคือฟิลาเมนต์ (filament) ซึ่งเป็น เส้นในสามมิติที่เชื่อมต่อระหว่างหัวสไปรอลในชั้นที่อยู่ติดกัน การเคลื่อนที่ของฟิลาเมนต์จะซับซ้อนตาม ความโค้ง (curvature) และการบิด (twist) ของฟิลาเมนต์ [16] ตัวอย่างรูปแบบของฟิลาเมนต์อย่างง่าย (รูป ที่ 2.1 ง-จ) คือ เส้นตรงและวงกลม อนึ่ง คลื่นสกอล์ที่มีฟิลาเมนต์เป็นวงนั้น นิยมเรียกว่าสกอล์ริง (scroll ring) [16]

คลื่นสกอล์ได้รับความสนใจเป็นอย่างมาก เนื่องจาก มีการทดลองโดยใช้เนื้อเยื่อหัวใจจากสัตว์ที่ สนับสนุนว่า คลื่นสกอล์เป็นสาเหตุของโรคหัวใจบางชนิด [17] กล่าวคือ โดยปกติแล้วคลื่นศักย์ไฟฟ้าซึ่งทำ ให้เนื้อเยื่อหัวใจหดและขยายเพื่อสูบฉีดโลหิตมีรูปแบบเป็นส่วนหนึ่งของคลื่นทรงกลม (truncated spherical Wave) แต่หากหัวใจมีความผิดปรกติบางอย่างจนทำให้คลื่นศักย์ไฟฟ้าดังกล่าวเปลี่ยนรูปแบบเป็นคลื่นสกอล์ หัวใจจะเต้นเร็วขึ้นตามความถี่ของคลื่นสกอล์และประสิทธิภาพการสูบฉีดโลหิตจะลดลง (tachycardia) หาก คลื่นสกอล์นั้นแตกออกเป็นคลื่นสกอล์ย่อยๆ เกิดเป็นความโกลาหลของศักย์ไฟฟ้า (electrical turbulence) จะทำให้เนื้อเยื่อหัวใจแต่ละส่วนหดขยายไม่ประสานกัน (fibrillation) และไม่สามารถสูบฉีดโลหิตได้เลย

ศาสตราจารย์วินฟรี (A.T. Winfree) ได้รายงานผลวิจัย [18] ที่ใช้แผ่นเนื้อเยื่อหัวใจว่า พบการ เปลี่ยนรูปของคลื่นสไปรอลที่ผิวเนื้อเยื่อเป็นคลื่นโกลาหลเมื่อแผ่นเนื้อเยื่อนั้นหนากว่าค่าจำกัดค่าหนึ่ง ดังนั้น ปรากฏการณ์นี้เกิดขึ้นเฉพาะในตัวกลางสามมิติเท่านั้น (จวบจนปัจจุบัน วิธีสังเกตการณ์สามมิติเต็มรูปแบบ ของคลื่น ไฟฟ้าในเนื้อเยื่อหัวใจยังคงอยู่ในขั้นพัฒนา [19]) ในภายหลังนักวิจัยได้ขนามนามว่าปรากฏการณ์ คลื่นโกลาหลของวินฟรี (Winfree turbulence) เนื่องด้วยผลกระทบโดยตรงต่อมนุษย์นี้ นักวิทยาศาสตร์ จำนวนมากได้ทุ่มเทวิจัยในด้านการควบคุมคลื่นทั้งในตัวกลางสองและสามมิติ รวมทั้งการระงับความ โกลาหลของคลื่น ในช่วงสองทศวรรษที่ผ่านมา [20]



รูปที่ 2.1 ตัวอย่างคลื่นสไปรอล (ก) ในตัวกลางปฏิกิริยาบิโลซอฟ-ซาบอทินสกี [2] (ข) คลื่นออกซิเดชันของ คาร์บอนมอนอกไซด์บนผิวทองคำขาว [3] (ค) คลื่นการรวมตัวกันของราเมือก [5] คลื่นสกอล์ซึ่งเปรียบได้กับ การนำคลื่นสไปรอลมาซ้อนต่อกัน เช่น (ง) คลื่นสกอล์ซึ่งมีฟิลาเมนต์เป็นเส้นตรง [21] และ (จ) สกอล์ริงมีฟิลาเมนต์เป็นวง [22]

# การควบคุมคลื่นด้วยสนามไฟฟ้า

การศึกษาผลของสนามไฟฟ้าต่อคลื่นทั้งในตัวกลางเคมีและในการจำลองแบบทางคอมพิวเตอร์นั้น พบว่า สนามไฟฟ้ามีผลให้หัวสไปรอลเคลื่อนที่เป็นเส้นตรงทำมุมกับสนามไฟฟ้า โดยอัตราเร็วและขนาดของ มุมขึ้นกับความแรงของสนามไฟฟ้า [13,14] ผลการจำลองแบบทางคอมพิวเตอร์อีกฉบับหนึ่ง [23] ได้แสดง ว่า เมื่อกำหนดให้สนามไฟฟ้าคงที่ อัตราเร็วและขนาดของมุมดังกล่าวขึ้นกับสภาพกระตุ้นได้ของตัวกลาง ผลของสนามไฟฟ้าต่อคลื่นในสามมิตินั้นขึ้นกับรูปร่างของฟิลาเมนต์ เช่น ในบทความของนักวิจัยที่ปรึกษา และคณะได้รายงานว่า วงฟิลาเมนต์จะเคลื่อนที่สวนทางกับทิศของสนามไฟฟ้าและขณะเดียวกันแรงจาก สนามไฟฟ้ามีผลให้ระนาบของฟิลาเมนต์จัดเรียงตัวใหม่ (reorientation) [24,25] หากฟิลาเมนต์เป็นเส้นตรง ฟิลาเมนต์จะเคลื่อนที่ภายใต้สนามไฟฟ้าเช่นเดียวกับกรณีของหัวสไปรอล [26]

อนึ่ง การเคลื่อนที่ของคลื่นสกอล์สามารถควบคุมได้ด้วยปัจจัยภายนอกอื่นๆ เช่น เกรเดียนท์แสง (light gradient) [27,28] (เมื่อใช้ตัวกลางเคมีที่ไวต่อแสง) และ เกรเดียนท์อุณหภูมิ (temperature gradient) [29,30] ในโครงการวิจัยที่เสนอนี้ได้เลือกใช้สนามไฟฟ้าที่สม่ำเสมอทั้งตัวกลางเคมีเป็นปัจจัยภายนอก (ซึ่ง สามารถทำได้ง่ายดังที่รายงานในวิทยานิพนธ์ [31]) เพื่อให้การวิเคราะห์ การวิจารณ์ และการสรุปผลการ ทดลองเป็นไปอย่างชัดเจน ในขณะที่การควบคุมด้วยแสงหรืออุณหภูมินั้น เกรเดียนท์จะเปลี่ยนตามตำแหน่ง ในตัวกลางและมีผลให้การเคลื่อนที่ของคลื่นสกอล์ซับซ้อนมากขึ้น [32]

# 3. ระเบียบวิธีวิจัย

# การเตรียมตัวกลางเคมีในลักษณะวุ้น

ตัวกลางเคมีที่จะใช้ประกอบด้วยสารตั้งต้นดังนี้ แฟโรอีน (ferroin) กรดซัลฟูริค (H<sub>2</sub>SO<sub>4</sub>) โปแต สเซียมโบรเมท (KBrO<sub>3</sub>) และ กรดมาโลนิค (Malonic acid) เพื่อความสะดวก สารตั้งต้นนี้จะถูกเตรียมไว้ใน รูปสารละลายเข้มข้น (stock solution) เพื่อใช้สำหรับการทดลองในช่วงประมาณสองสัปดาห์

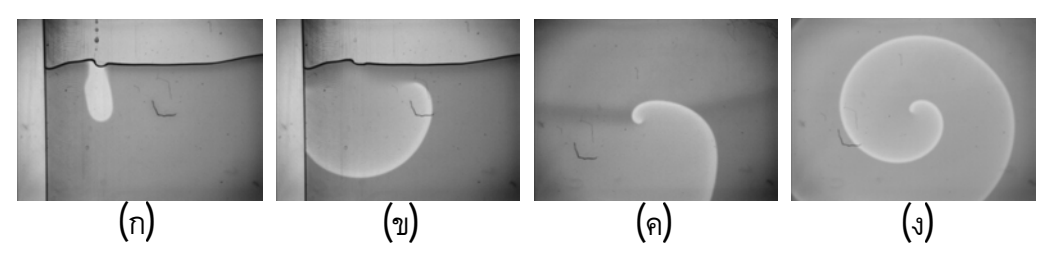
ตัวกลางเคมีจะถูกเตรียมในลักษณะวุ้น (agar gel) เพื่อป้องกันการรบกวนจากพลศาสตร์ของไหล (hydrodynamic perturbation) ซึ่งเกิดขึ้นในตัวกลางเคมีที่เป็นของเหลว โดยความเข้มข้นวุ้นประมาณ 0.5-1% โดยมวล ขั้นตอนการเตรียมตัวกลางมีดังนี้

- 1. ตัมผงวุ้นกับน้ำจนเดือด เพื่อให้ผงวุ้นละลายหมด
- 2. เติมน้ำส่วนที่หายไปเนื่องจากการระเหยในระหว่างที่รอให้น้ำวุ้นเย็นลงที่ประมาณ  $40^{\circ}\mathrm{C}$
- 3. ผสมสารตั้งต้นกับน้ำวุ้นในอัตราส่วนที่ได้คำนวณไว้ก่อนแล้วเพื่อให้ได้ความเข้มข้นของสารใ ตัวกลางตามที่ต้องการ เมื่อเสร็จขั้นตอนนี้แล้ว อุณหภูมิของตัวกลางมีค่าประมาณ 35°C ตัวกลางนี้จะถูกใช้ทันทีในขั้นตอนการสร้างคลื่น เนื่องจากวุ้นจะจับตัวที่อุณหภูมิต่ำกว่า 30°C

## การสร้างคลื่น

การสร้างคลื่นทั้งในตัวกลางสองมิติและสามมิติใช้หลักการเดียวกัน คือ การทำให้เกิดหน้าคลื่น ปลายเปิดในตัวกลาง ในตัวกลางที่บางมากจุดปลายเปิดนี้จะขดเป็นคลื่นสไปรอล ในโครงการนี้จะใช้เทคนิค การเติมสารสองชั้น (two-layer strategy) ขั้นตอนมีดังนี้

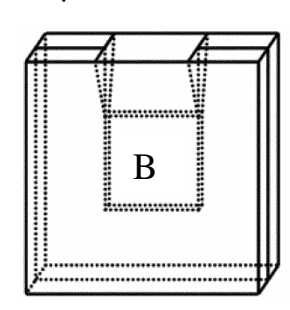
- 1. เติมสารชั้นแรกประมาณครึ่งความสูงของภาชนะบรรจุตัวกลางเคมี (reactor)
- 2. จุ่มลวดเงิน (silver wire) ลงในสารชั้นแรกเพื่อกระตุ้นให้เกิดคลื่นรอบ ๆลวดเงิน (รูปที่ 3.1ก) หน้าคลื่นจะแผ่ออกจากจุดเริ่มต้น และที่ผิวบนของสารชั้นแรกจะเกิดเป็นหน้าคลื่นปลายเปิดซึ่ง เป็นจุดในตัวกลางสองมิติ (รูปที่ 3.1ข)
- 3. เติมสารชั้นที่สองลงบนสารชั้นแรก หน้าคลื่นปลายเปิดจากสารชั้นแรกจะเคลื่อนที่เข้าสู่สารชั้นที่ สอง (รูปที่ 3.1ค) และจะขดเกิดเป็นคลื่นสไปรอล (รูปที่ 3.1ง)



รูปที่ 3.1 การสร้างคลื่นสไปรอลในตัวกลางเคมีสองมิติ [10] ในตัวกลางเคมีนี้หน้าคลื่นมีสีฟ้าขณะที่บริเวณ อื่นมีสีแดง (ก) คลื่นถูกกระตุ้นด้วยลวดเงิน (ข) คลื่นปลายเปิดในสารชั้นแรก (ค) คลื่นเคลื่อนที่เข้าสู่สารชั้นที่ สองและขดเป็น (ง) คลื่นสไปรอล

# ภาชนะบรรจุตัวกลางเคมี

ภาชนะบรรจุตัวกลางเคมี (reactor) มีลักษณะใส ทำจากพลาสติกทนกรด



รูปที่ 3.2 ร่างภาชนะบรรจุตัวกลางเคมี (reactor) สำหรับการทดลองสองมิติ ปริมาตรบรรจุตัวกลาง (BZ) มีขนาด  $4 \times 4$  ซม.  $^2$  หนาไม่เกิน 1 มม. [10]

### การป้อนสนามไฟฟ้า

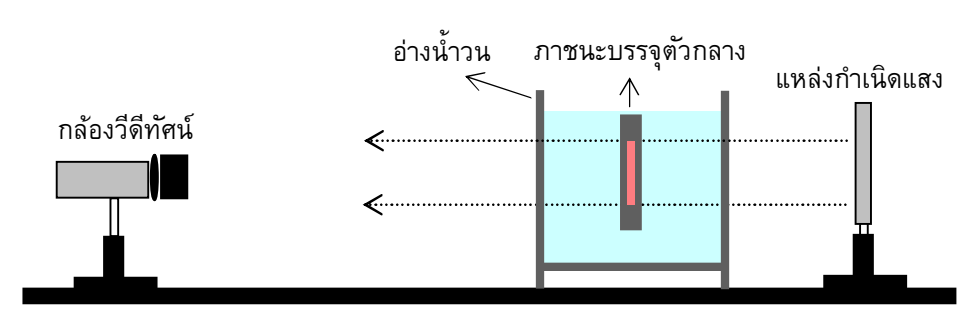
ในการทดลองผลของสนามไฟฟ้าต่อคลื่นสไปรอลนั้นจะใช้แหล่งกำเนิดไฟฟ้ากระแสตรงในโหมด กระแสคงที่ (current constant mode) โดยจุ่มขั้วไฟฟ้าทำจากสแตนเลสลงในอ่างอิเล็กโตรไลต์ เพื่อป้องกัน การเจือปน สารอิเล็กโตรไลต์จึงทำจากสารละลายเคมี (ลักษณะเหลวไม่มีส่วนผสมของวุ้น) ซึ่งมีความเข้มข้น ของสารตั้งต้นเช่นเดียวกับในตัวกลางเคมีซึ่งมีลักษณะเป็นวุ้น ในขณะทำการทดลองจะเกิดก๊าซที่ขั้วไฟฟ้า ซึ่งสามารถระบายออกทางปล่องได้

# การควบคุมอุณหภูมิด้วยอ่างน้ำวน

เนื่องจากอุณหภูมิมีผลต่อสมบัติของคลื่นในตัวกลางนี้ เช่น อัตราเร็ว คาบเวลา ความถี่ เป็นต้น อีกทั้ง การป้อนกระแสไฟฟ้า (เพื่อสร้างสนามไฟฟ้า) ให้กับตัวกลางในบางการทดลองมีผลให้เกิดความร้อนใน ตัวกลาง ในทุกการทดลองจึงมีการควบคุมอุณหภูมิของตัวกลางโดยจัดตั้งภาชนะที่บรรจุตัวกลางเคมีลงใน อ่างน้ำวน อุณหภูมิของตัวกลางจะถูกควบคุมไว้ที่ 25°C อ่างนี้ทำจากพลาสติกใส ลักษณะเป็นกล่อง ลูกบาศก์ผิวเรียบเพื่ออำนวยความสะดวกแก่การบันทึกผลการทดลองผ่านกล้องวีดีทัศน์

# ชุดทดลองและการบันทึกผลการทดลอง

รูปที่ 3.3 แสดงร่างชุดทดลองสำหรับการทดลองคลื่นสองมิติ การบันทึกผลการทดลองเริ่มจาก แหล่งกำเนิดแสงขาวจากแผงหลอดฟลูออเรสเซนต์ส่องผ่านแผ่นแก้วฝ้า (milky glass) ซึ่งทำให้ความเข้ม แสงสม่ำเสมอขึ้น จากนั้นแสงจะเดินทางผ่านอ่างน้ำวนและภาชนะบรรจุตัวกลางเคมี (รูปที่ 3.2) ไปยังกล้องวี ดีทัศน์ สัญญาณจากกล้องวีดีทัศน์จะถูกแปลงเป็นภาพดิจิตัลขาวดำ (gray scale) ก่อนบันทึกลงในเครื่อง คอมพิวเตอร์



รูปที่ 3.3 ร่างชุดทดลองสำหรับการทดลองสองมิติ [10]

# การวิเคราะห์ผลการทดลอง

เนื่องจากอัตราเร็วหน้าคลื่นในตัวกลางที่ถูกกระตุ้นได้แปรผกผันกับความโค้งของหน้าคลื่น โดยเฉพาะหน้าคลื่นที่อยู่ใกล้หัวสไปรอล คลื่นจึงเคลื่อนที่เร็วขึ้นตามระยะห่างจากหัวสไปรอล (ความโค้ง ลดลง) สำหรับหน้าคลื่นที่อยู่ห่างจากหัวสไปรอลมากกว่าหนึ่งความยาวคลื่นอัตราเร็วมีค่าคงที่โดยประมาณ (ความโค้งเปลี่ยนแปลงน้อยมาก) ในงานวิจัยนี้จะวัดความยาวคลื่นและคาบเวลาในบริเวณที่ห่างจากหัวสไป รอลประมาณหนึ่งถึงสองความยาวคลื่น และคำนวณอัตราเร็วหน้าคลื่นจากผลหารของความยาวคลื่นและ คาบเวลา

### การจำลองแบบทางคอมพิวเตอร์

สนามไฟฟ้ามีผลต่อคลื่นในตัวกลางเคมีที่ใช้เนื่องจากในตัวกลางนี้ประกอบด้วยไอออนจำนวนมาก ซึ่ง ผลของสนามไฟฟ้าสามารถจำลองแบบทางคอมพิวเตอร์โดยใช้กลไกปฏิกิริยาและการแพร่ผนวกกับเทอม เกรเดียนท์ในทิศตรงข้ามกับสนามไฟฟ้า ในกรณีการป้อนสนามไฟฟ้าขนาด E ในทิศ+x ความเข้มข้นของ ตัวกระตุ้น u (activator) และ ตัวยับยั้ง v (inhibitor) เปลี่ยนแปลงตามเวลา t ดังนี้

$$\frac{\partial u}{\partial t} = \frac{1}{\varepsilon} \left( u - u^2 - f v \frac{u - q}{u + q} \right) + D_u \nabla^2 u - M_u E \frac{\partial u}{\partial x}$$

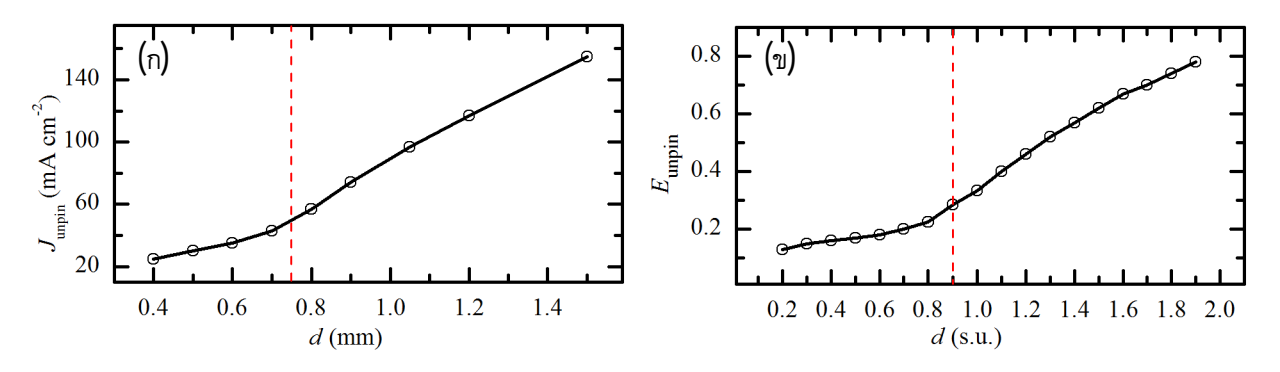
$$\frac{\partial v}{\partial t} = u - v + D_v \nabla^2 v - M_v E \frac{\partial v}{\partial x}$$

ค่าพารามิเตอร์ที่ให้วิถีหัวสไปรอลเป็นวงกลมเมื่อไม่มีสนามไฟฟ้า คือ  $\varepsilon=0.01$ , q=0.002, f=1.4 ค่า สัมประสิทธิ์การแพร่  $D_u=1$ ,  $D_v=0.6$  ส่วนค่าสภาพการเคลื่อนที่ของไอออน (ionic mobility) มีค่า  $M_u=-1.0~M_v=2.0$ 

จุดบกพร่องสำหรับตรึงคลื่นคือบริเวณที่คลื่นไม่สามารถเคลื่อนที่เข้าไปได้ ซึ่งจำลองโดยใช้หลักการ ของผนังที่สารผ่านไม่ได้ (no flux boundary) ในการจำลองแบบจะใช้วัตถุทรงกระบอกขนาดต่างๆกัน เพื่อ ตรึงคลื่นเช่นเดียวกับที่ใช้ในการทดลอง

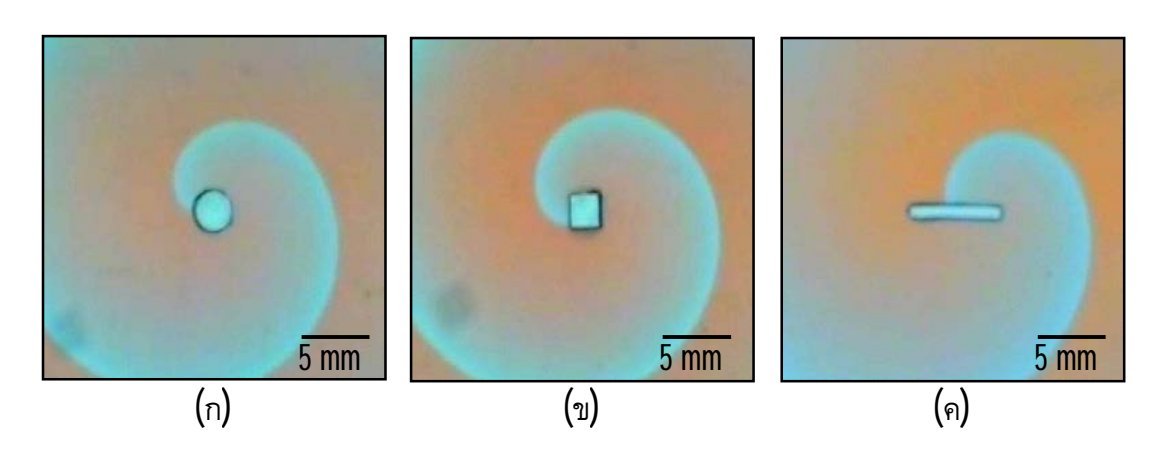
### 4. ผลวิจัย

ผู้วิจัยพบว่า ผลของสิ่งกีดขวางต่อการเคลื่อนที่ของคลื่นสไปรอลในตัวกลางขึ้นกับระยะห่าง ระหว่างสิ่งกีดขวางกับหัวสไปรอล กรณีระยะห่างมีค่ามาก สไปรอลจะไม่ถูกรบกวน เมื่อระยะห่างลดลง สไป รอลจะถูกผลักออกห่างจากสิ่งกีดขวาง และ เมื่อระยะห่างมีค่าน้อยมากกว่าค่าวิกฤติ สไปรอลจะถูกดึงดูดจน หัวสไปรอลถูกตรึงกับสิ่งกีดขวาง สิ่งกีดขวางดังกล่าวส่งผลต่อสมบัติของหน้าคลื่นที่ห่างออกไป กล่าวคือ ความยาวคลื่น คาบเวลา และอัตราเร็วของคลื่น เพิ่มขึ้นตามขนาดของสิ่งกีดขวาง ในส่วนการทดลองตรึง คลื่นสไปรอลและปลดปล่อยคลื่นที่ถูกตรึงด้วยกระแสไฟฟ้าในตัวกลางปฏิกิริยาบิโลซอฟ-ซาบอทินสกี ผู้วิจัย ได้มุ่งเน้นการสร้างคลื่นสไปรอลให้อยู่ใกลักับสิ่งกีดขวางซึ่งทำจากพลาสติกทรงกระบอกเส้นผ่านศูนย์กลาง 0.4-1.5~mm และทำการตรึงคลื่นสไปรอลได้สำเร็จ จากนั้นจึงทดลองป้อนกระแสไฟฟ้ามีค่าสูงเกินค่าวิกฤติ คลื่นสไปรอลจะหลุดและเคลื่อนที่ห่างจากสิ่งกีดขวางได้ เมื่อความหนาแน่นกระแสไฟฟ้ามีค่ามากพอคือ  $J_{\text{unpin}}$ , หัวสไปรอลซึ่งถูกตรึงด้วยสิ่งกีดขวางวงกลมจะถูกตึงออกและเลื่อนห่างออกจากสิ่งกีดขวาง โดยค่า วิกฤติ  $J_{\text{unpin}}$  มีขนาดเพิ่มขึ้นตามขนาดเส้นผ่านศูนย์กลางของสิ่งกีดขวาง d อีกทั้งอัตราการเพิ่ม  $\Delta J_{\text{unpin}}/\Delta d$  มีค่ามากสำหรับสิ่งกีดขวางที่มีขนาดใหญ่กว่าแกนของสไปรอล ดังแสดงในรูปที่ 4.1



รูปที่ 4.1 ความสัมพันธ์ระหว่างสนามไฟฟ้าวิกฤติสำหรับการกำจัดคลื่นสไปรอลออกจากจุดตรึงและเส้นผ่าน ศูนย์กลางของสิ่งกีดขวางใน (ก) การทดลองกับตัวกลางเคมี และ (ข) การจำลองแบบทาง คอมพิวเตอร์ เส้นประแสดงขนาดของแกนสไปรอล

คณะผู้วิจัยได้ใช้แสงเลเซอร์ตัดแผ่นพลาสติกใสหนา 1 มิลลิเมตร เพื่อใช้เป็นสิ่งกีดขวางที่มีรูปทรง ต่างกัน ประกอบด้วย วงกลม สี่เหลี่ยมจตุรัส และสี่เหลี่ยมผืนผ้าที่มีความยาวและความกว้างต่าง ๆกัน แต่สิ่ง กีดขวางทั้งหมดมีขนาดพื้นที่ (area) ใกล้เคียงกัน คือ ประมาณ 6.0 ± 0.2 mm² เนื่องจากสิ่งกีดขวางมี รูปทรงที่ต่างกันจึงทำให้มีขนาดเส้นรอบวง (circumference) ต่างกัน จากนั้นผู้วิจัยได้ทำการทดลองตรึงคลื่น สไปรอลในตัวกลางเคมีกับสิ่งกีดขวางดังกล่าวได้สำเร็จดังแสดงในรูปที่ 4.2

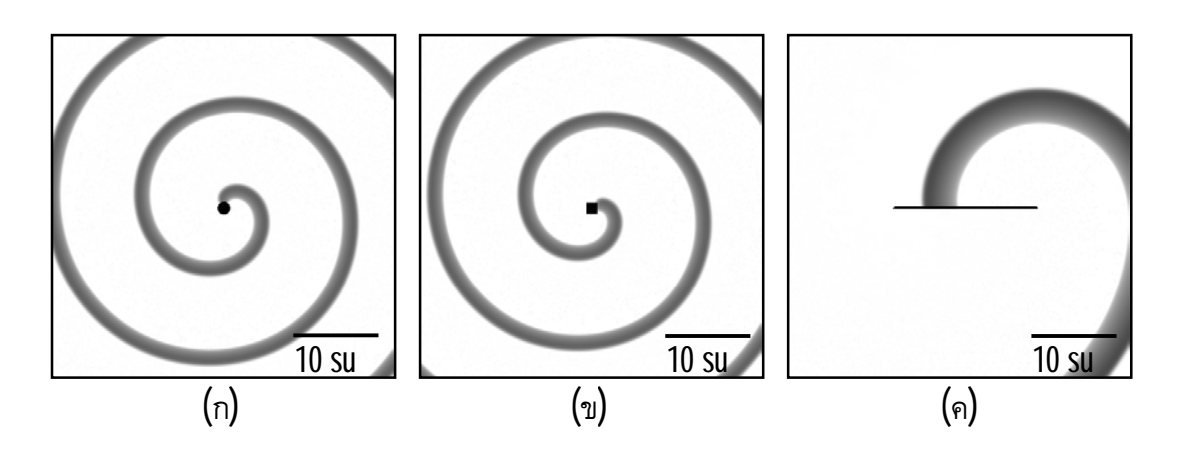


รูปที่ 4.2 ตัวอย่างคลื่นสไปรอลที่ถูกตรึงไว้กับสิ่งกีดขวางพลาสติกรูปทรงต่างๆ คือ (ก) วงกลมขนาดเส้น ผ่านศูนย์กลาง 2.8 มิลลิเมตร (ข) สี่เหลี่ยมผืนผ้าขนาด 2.3 มิลลิเมตร  $\times$  2.6 มิลลิเมตร และ (ค) สี่เหลี่ยมผืนผ้าขนาด 0.9 มิลลิเมตร  $\times$  0.5 มิลลิเมตร

ผลการวิเคราะห์พบว่าสมบัติของคลื่นสไปรอลเปลี่ยนตามขนาดเส้นรอบวงของสิ่งกีดขวาง กล่าวคือ สิ่งกีดขวางที่มีเส้นรอบวงยาวขึ้นทำให้คาบเวลา (period) ความยาวคลื่น (wavelength) และอัตราเร็ว (velocity) ของคลื่นสไปรอลที่วนรอบสิ่งกีดขวางนั้นเพิ่มขึ้น ดังตารางที่ 4.1 จากนั้นผู้วิจัยได้ป้อน กระแสไฟฟ้าให้กับตัวกลางเคมีเพื่อบังคับให้หัวของคลื่นสไปรอลหลุดออกจากสิ่งกีดขวางและเลื่อนไปยัง ขอบตัวกลาง และเมื่อหัวของสไปรอลชนกับขอบตัวกลางคลื่นสไปรอลจะถูกกำจัดออกจากตัวกลาง ค่า กระแสไฟฟ้าวิกฤติ (J<sub>unpin</sub>) เพิ่มขึ้นตามขนาดเส้นรอบวงของสิ่งกีดขวางดังตารางที่ 4.1

ตารางที่ 4.1 แสดงสมบัติของคลื่นสไปรอลที่ถูกตรึงด้วยสิ่งกีดขวางที่มีรูปทรงต่างกันและค่าความหนาแน่น กระแสไฟฟ้าวิกฤติสำหรับกำจัดคลื่นในตัวกลางเคมี

obstacle	area (mm²)	circumference (mm)	wavelength (mm)	period (min)	velocity (mm/min)	$J_{unpin}$ (mA/cm <sup>2</sup> )
no obstacle	-	-	7.47	11.42	0.65	-
circle, ∅ = 2.8 mm	6.2	8.8	12.44	17.33	0.72	60
rectangle, 2.3 mm $\times$ 2.6 mm	6.0	9.8	12.38	16.45	0.75	65
rectangle, 1.3 mm $\times$ 4.6 mm	6.0	11.8	15.88	19.67	0.81	116
rectangle, 1.2 mm $\times$ 4.9 mm	5.9	12.2	15.50	19.06	0.80	123
rectangle, 0.9 mm $\times$ 6.5 mm	5.9	14.8	18.75	22.81	0.83	160



รูปที่ 4.3 ตัวอย่างคลื่นสไปรอลที่ถูกตรึงไว้กับสิ่งกีดขวางรูปทรงต่างๆ ในแบบจำลองทางคอมพิวเตอร์ (ก) วงกลมขนาดเส้นผ่านศูนย์กลาง  $1.5~{
m SU}$  (ข) สี่เหลี่ยมจตุรัสขนาด  $1.3~{
m SU} imes 1.3~{
m SU}$  และ (ค) สี่เหลี่ยมผืนผ้า ขนาด  $0.1~{
m SU} imes 17.0~{
m SU}$ 

คณะผู้วิจัยได้ทำการปรับปรุงโปรแกรมสำหรับการจำลองแบบทางคอมพิวเตอร์เพื่อศึกษาผลของรูป ทรงสิ่งกีดขวางต่อการเคลื่อนที่ของคลื่นสไปรอลที่ถูกตรึงไว้ โดยได้ทดลองตรึงคลื่นสไปรอลด้วยสิ่งกีดขวาง รูปทรงต่าง ๆกัน คือ วงกลม สี่เหลี่ยมจตุรัส และสี่เหลี่ยมผืนผ้าที่มีด้านกว้างและยาวหลายขนาด ทั้งนี้สิ่งกีดขวางทั้งหมดมีขนาดพื้นที่ใกล้เคียงกัน คือ ประมาณ 1.70 ± 0.04 SU จากนั้นผู้วิจัยได้ ทำการตรึงคลื่นสไปรอลกับสิ่งกีดขวางดังกล่าว ดังแสดงในรูปที่ 4.3

ผลการวิเคราะห์พบว่าสมบัติของคลื่นสไปรอลเปลี่ยนตามขนาดเส้นรอบวงของสิ่งกีดขวาง เช่นเดียวกับผลจากการทดลองตัวกลางเคมี กล่าวคือ สิ่งกีดขวางที่มีเส้นรอบวงยาวขึ้นทำให้คาบเวลา (period) ความยาวคลื่น (wavelength) และอัตราเร็ว (velocity) ของคลื่นสไปรอลที่วนรอบสิ่งกีดขวางนั้น เพิ่มขึ้น ดังตารางที่ 4.2 จากนั้นผู้วิจัยได้ป้อนกระแสไฟฟ้าให้กับตัวกลางเคมีเพื่อบังคับให้หัวของคลื่น สไปรอลหลุดออกจากสิ่งกีดขวางและเลื่อนไปยังขอบตัวกลาง และเมื่อหัวของสไปรอลชนกับขอบตัวกลาง คลื่นสไปรอลจะถูกกำจัดออกจากตัวกลาง ค่ากระแสไฟฟ้าวิกฤติ (J<sub>unpin</sub>) เพิ่มขึ้นตามขนาดเส้นรอบวงของสิ่ง กีดขวางดังตารางที่ 4.2

ตารางที่ 4.2 แสดงสมบัติของคลื่นสไปรอลที่ถูกตรึงด้วยสิ่งกีดขวางที่มีรูปทรงต่างกันและค่าความหนาแน่น กระแสไฟฟ้าวิกฤติสำหรับกำจัดคลื่นในการจำลองแบบทางคอมพิวเตอร์

obstacle	area	circumference	wavelength	period	velocity	J <sub>unpin</sub>
	(su²)	(su)	(su)	(tu)	(su/tu)	(au)
no obstacle	-	-	10.00	1.50	6.67	-
circle, ∅ = 1.5 su	1.77	4.7	10.70	1.56	6.86	0.62
square, $1.3 \text{ su} \times 1.3 \text{ su}$	1.69	5.2	10.80	1.58	6.86	0.68
rectangle, 1.0 su $\times$ 1.7 su	1.70	5.4	10.90	1.58	6.92	0.70
rectangle, 0.5 su $\times$ 3.4 su	1.70	7.8	12.60	1.68	7.50	0.91
rectangle, $0.3 \text{ su} \times 5.4 \text{ su}$	1.62	11.4	15.40	1.86	8.28	1.24
rectangle, 0.2 su $\times$ 8.5 su	1.70	17.4	20.70	2.16	9.58	1.66
rectangle, 0.1 su $\times$ 17.0 su	1.70	34.2	36.70	3.02	12.17	2.16

su: system unit, tu: time unit, au: arbitrary unit

## 5. เอกสารอ้างอิง

- [1] A.M. Turing. The chemical basis of morphogenesis. *Phil. Trans. Roy. Soc. Lond. B*, **237**:37-72, 1952.
- [2] A.T. Winfree. Spiral waves of chemical activity. *Science*, **175**:634-636, 1972.
- [3] S. Nettesheim, A. von Oertzen, H.H. Rotermund, and G. Ertl. Reaction diffusion patterns in the catalytic CO-oxidation on Pt(110): Front propagation and spiral waves. J. Chem. Phys., 98:9977-9985, 1993.
- [4] Website. http://nobelprize.org/nobel\_prizes/chemistry/laureates/2007
- [5] F. Siegert and C.J. Weijer. Digital image processing of optical density wave propagation in dictyostelium discoideum. *J. Cell Sci*, **93**:325-335, 1989.
- [6] B.P. Belousov. A periodic reaction and its mechanism, In Sbornik Referatov po Radiatsionni Meditsine. *Moscow: Medgiz*, pages 145-147, 1958.
- [7] A.M. Zhabotinsky. Periodic process of the oxidation of malonic acid in solution (study of the kinetics of Belosouv's reaction). *Biofizika*, **9**:306-311, 1964.
- [8] T. Plesser, S.C. Müller, and B. Hess. Spiral wave dynamics as a function of proton concentration in the ferroin-catalyzed Belousov-Zhabotinsky reaction. *J. Phys. Chem.*, **94**:7501-7507, 1990.
- [9] G. Li, Q. Ouyang, V. Petrov, and H.L. Swinney. Transition from simple rotating chemical spirals to meandering and traveling spirals. *Phys. Rev. Lett.*, **77**:2105-2108, 1996.
- [10] C. Luengviriya, U. Storb, M.J.B. Hauser, and S.C. Müller. An elegant method to study an isolated spiral wave in a thin layer of a batch Belousov-Zhabotinsky reaction under oxygen-free conditions. *Phys. Chem. Chem. Phys.*, **8**:1425, 2006.
- [11] O. Kheowan and S.C. Müller. Control of spiral waves in excitable media. *J.Appl. Math. Comp.*, **164**:373-390, 2005
- [12] O. Kheowan, C. Chan, V.S. Zykov, O. Rangsiman, and S.C. Müller. Spiral wave dynamics under feedback derived from a confined circular domain. *Phys. Rev. E*, **64**:03520, 2001.

- [13] O. Steinbock, J. Schütze, and S.C. Müller. Electric-field-induced drift and deformation of spiral waves in an excitable medium. *Phys. Rev. Lett.*, **68**:248-251, 1992.
- [14] J. Schütze, O. Steinbock, and S.C. Müller. Forced vortex interaction and annihilation in an active medium. *Nature*, **356**:45-46, 1992.
- [15] A.T. Winfree. Scroll-shaped waves of chemical activity in three dimensions. *Science*, **181**:937-939, 1973.
- [16] J.J. Tyson and S.H. Strogatz. The differential geometry of scroll waves. *Int. J. Bif. Chaos*, **1**:723-744, 1991.
- [17] V.I. Krinsky, V.N. Biktashev, and A.M. Pertsov. Autowave approachs to the cessation of autowave arrhythmias. *Ann. N. Y. Acad. Sci.*, **591**:232-246, 1990.
- [18] A.T. Winfree. Electrical turbulence in three-dimensional heart muscle. *Science*, **266**:1003-1006, 1994.
- [19] E.M. Cherry and F.H. Fenton. Visualization of spiral and scroll waves in simulated and experimental cardiac tissue. *New J. Phys.*, **10**:125016, 2008.
- [20] A.S. Mikhailov and K. Showalter. Control of waves, patterns and turbulence in chemical systems. *Phys. Rep.*, **425**:79-194, 2006.
- [21] U. Storb, C.R. Neto, M. Bär, and S.C. Müller. A tomographic study of desynchronization and complex dynamics of scroll waves in an excitable chemical reaction with a gradient. *Phys. Chem. Chem. Phys.*, **5**:2344-2353, 2003.
- [22] S. Alonso and A.V. Panfilov. Negative filament tension in the Luo-Rudy model of cardiac tissue. *Chaos*, **17**:015102, 2007.
- [23] H. Henry. Spiral wave drift in an electric field and scroll wave instabilities. *Phys. Rev. E*, **70**:026204, 2004.
- [24] C. Luengviriya, S.C. Müller, and M.J.B. Hauser. Reorientation of scroll rings in an advective field. *Phys. Rev. E*, **77**:015201(R), 2008.
- [25] C. Luengviriya and M.J.B. Hauser. Stability of scroll ring orientation in an advective field. *Phys. Rev. E*, **77**: 056214, 2008.
- [26] C. Luengviriya. Dynamics of three-dimensional excitation waves. Otto-von-Guericke-Universität Magdeburg, thesis, page 95, 2008.
- [27] T. Amemiya, P. Kettunen, S. Kadar, T. Yamaguchi, and K. Showalter. Formation and evolution of scroll waves in photosensitive excitable media. *Chaos*, **8**:872-878, 1998.
- [28] T. Amemiya, S. Kadar, P. Kettunen, and K. Showalter. Spiral wave formation in three-dimensional excitable media. *Phys. Rev. Lett*, **77**:3244-3247, 1996.
- [29] A.M. Pertsov, R.R. Aliev, and V.I. Krinsky. Three-dimensional twisted vortices in an excitable chemical medium. *Nature*, **345**:419-421, 1990.
- [30] M. Vinson, S. Mironov, S. Mulvey, and A.M. Pertsov. Control of spatial orientation and lifetime of scroll rings in excitable media. *Nature*, **386**:477-480, 1997.
- [31] C. Luengviriya. Dynamics of three-dimensional excitation waves. Otto-von-Guericke-Universität Magdeburg, thesis, page 91, 2008.
- [32] M. Vinson and A.M. Pertsov. Dynamics of scroll rings in a parameter gradient. *Phys. Rev. E*, **59**:2764-2771, 1999.
- [33] C. Luengviriya, J. Luengviriya, M. Sutthiopad, P. Porjai, B. Tomapatanaget, S. C. Müller. Excitability of the Ferroin-Catalyzed Belousov–Zhabotinsky Reaction with Pyrogallol. *Chem. Phys. Lett.*, **561-562**:170–174, 2013.

### 6. ผลผลิตจากโครงการวิจัย

## 6.1 ผลงานตีพิมพ์ในวารสารวิชาการนานาชาติ

ผลการวิจัยจากโครงการนี้ได้รับการตีพิมพ์ในวารสารวิชาการนานาชาติ Physical Review E เป็น จำนวน 2 ฉบับ ในชื่อเรื่อง

- 1. M. Sutthiopad, J. Luengviriya, P. Porjai, B. Tomapatanaget, S. C. Müller, and **C. Luengviriya\***. Unpinning of Spiral Waves by Electrical Forcing in Excitable Chemical Media. *Phys. Rev. E*, **89**: 052902, 2014. IF: 2.313.
- 2. M. Sutthiopad, J. Luengviriya, P. Porjai, M. Phantu, J. Kanchanawarin, S. C. Müller, and **C. Luengviriya\***. Propagation of spiral waves pinned to circular and rectangular obstacles. *Phys. Rev. E*, **91**: 052912, 2015. IF: 2.326.

### 6.2 การนำผลงานวิจัยไปใช้ประโยชน์

โครงการวิจัยนี้มีส่วนช่วยผลิตนักวิทยาศาสตร์รุ่นใหม่ วิทยานิพนธ์ระดับปริญญาโทและปริญญาเอกรวม 2 ท่าน โดยงานวิจัยที่นิสิตได้รับมอบหมายเป็น

#### ภาคผนวก

ผลการวิจัยที่เผยแพร่ในวารสารวิชาการนานาชาติ Physical Review E จำนวน 2 ฉบับ ในชื่อเรื่อง

- 1. M. Sutthiopad, J. Luengviriya, P. Porjai, B. Tomapatanaget, S. C. Müller, and **C. Luengviriya\***. Unpinning of Spiral Waves by Electrical Forcing in Excitable Chemical Media. *Phys. Rev. E*, **89**: 052902, 2014. IF: 2.313.
- 2. M. Sutthiopad, J. Luengviriya, P. Porjai, M. Phantu, J. Kanchanawarin, S. C. Müller, and **C. Luengviriya\***. Propagation of spiral waves pinned to circular and rectangular obstacles. *Phys. Rev. E*, **91**: 052912, 2015. IF: 2.326.

#### Unpinning of spiral waves by electrical forcing in excitable chemical media

Malee Sutthiopad, <sup>1</sup> Jiraporn Luengviriya, <sup>2,3</sup> Porramain Porjai, <sup>1</sup> Boosayarat Tomapatanaget, <sup>4</sup> Stefan C. Müller, <sup>5</sup> and Chaiya Luengviriya<sup>1,\*</sup>

<sup>1</sup>Department of Physics, Kasetsart University, 50 Phaholyothin Road, Jatujak, Bangkok 10900, Thailand <sup>2</sup>Department of Industrial Physics and Medical Instrumentation, King Mongkut's University of Technology North Bangkok, 1518 Pibulsongkram Road, Bangkok 10800, Thailand

<sup>3</sup>Lasers and Optics Research Group, King Mongkut's University of Technology North Bangkok, 1518 Pibulsongkram Road, Bangkok 10800, Thailand

<sup>4</sup>Department of Chemistry, Chulalongkorn University, Bangkok 10330, Thailand
<sup>5</sup>Institute of Experimental Physics, Otto-von-Guericke University Magdeburg, Universitätsplatz 2, D-39106 Magdeburg, Germany (Received 12 February 2014; published 8 May 2014)

We present experimental observations on the electrically forced release of spiral waves pinned to unexcitable circular obstacles in the Belosov-Zhabotinsky reaction. When the applied electric current density reaches the necessary current density  $J_{\rm unpin}$ , the spiral tip is detached and subsequently drifts away from the obstacle.  $J_{\rm unpin}$  is found to increase with the obstacle diameter d. The growth rate  $\Delta J_{\rm unpin}/\Delta d$  is much higher for obstacles larger than the free spiral core compared to that for smaller obstacles. The experimental findings are confirmed by numerical simulations using the Oregonator model. The results imply that it is more difficult to release spiral waves pinned to larger obstacles, especially when the obstacle size exceeds that of the free spiral core.

DOI: 10.1103/PhysRevE.89.052902 PACS number(s): 05.45.-a, 05.65.+b, 82.40.Ck, 82.40.Qt

#### I. INTRODUCTION

Spiral waves evolve in different excitable media, e.g., during CO oxidation on a platinum surface [1], cell aggregation in slime mold colonies [2], electrical wave propagation in cardiac tissues [3], and concentration waves in the Belousov-Zhabotinsky (BZ) reaction [4,5]. Such spiral patterns of electrical excitation in the heart and their instabilities are involved in causing certain types of cardiac arrhythmia, such as ventricular tachycardia and fibrillations [6,7], which can potentially lead to sudden cardiac death.

Annihilation of spiral waves is possible when the waves drift until they hit the boundary of the medium. Even though this drift and annihilation can occur naturally, spiral waves in cardiac tissues are often stabilized by being pinned to local heterogeneities (e.g., veins or scars), which act as obstacles [3]. Note that obstacles may either attract or repulse spiral waves depending on the distance between the spiral core centers and the obstacles [8,9]. Furthermore, it has been predicted [10,11] that obstacles cause the period of pinned spiral waves to increase with the obstacle size. A systematic study of pinned spiral waves in a thin layer of the photosensitive ruthenium-catalyzed BZ reaction [12] has revealed that wave period, wavelength, and velocity increase with the size of a circular unexcitable obstacle created by a laser spot. For threedimensional BZ media, spiral structures known as scroll rings are often observed to contract and eventually self-annihilate [13,14]. The intrinsic contraction is suppressed, when a scroll ring is pinned to an obstacle [15,16].

It has been demonstrated that low-energy shocks, produced by virtual electrode polarization [17], can unpin and terminate ventricular tachycardia in isolated rabbit ventricles [18] and cell cultures of neonatal rat ventricular myocytes [19,20]. Other low-energy methods use a high-frequency train of electrical stimuli to eliminate spiral waves in cardiac tissue cultures by inducing unpinning and drift of the waves, until they collide with the boundary of the medium [21,22]. Such an external wave train is used to release a spiral wave pinned to a cluster of small droplets of oil in the BZ reaction [23].

In this article, we present an investigation of the electrically forced unpinning of spiral waves in BZ media. In the absence of obstacles, an applied electrical current results in an advective motion of ionic species and induces a drift of the spiral tips along a straight path. The drift velocity is found to increase with the magnitude of applied current [24–26]. Our experiments are performed in uniform thin layers of the BZ reaction [27] using chemically inert plastic cylinders with well-defined diameters as unexcitable obstacles. Thus, the relation between the strength of forcing and the obstacle size is precisely specified. We perform simulations using the Oregonator model [28,29] in close correspondence with the experimental results.

#### II. EXPERIMENTS

#### A. Methods

The Belousov-Zhabotinsky (BZ) solutions are prepared from NaBrO<sub>3</sub>, H<sub>2</sub>SO<sub>4</sub>, malonic acid (MA) and ferroin, all purchased from Merck. Stock solutions of NaBrO<sub>3</sub> (1 M) and MA (1 M) are freshly produced by dissolving powder in deionized water (conductivity of ~0.056  $\mu$ S cm<sup>-1</sup>), whereas stock solutions of H<sub>2</sub>SO<sub>4</sub> (2.5 M) and ferroin (25 mM) are commercially available. To prevent any hydrodynamic perturbation, the reaction is embedded in a 1.0% wt/wt agarose gel (Sigma). Appropriate volumes of the stock solutions are mixed and diluted in deionized water to form BZ solutions with initial concentrations: [H<sub>2</sub>SO<sub>4</sub>] = 200 mM, [MA] = 50 mM, [NaBrO<sub>3</sub>] = 50 mM, and [ferroin] = 0.625 mM. The temperature is controlled at 24 °C  $\pm$  1 °C. In the absence of electrical forcing as well as any obstacle, these BZ media

<sup>\*</sup>Corresponding author: fscicyl@ku.ac.th

support rotating spiral waves, the tip of which (measured location as in Ref. [27]) moves around a circular area (i.e., the spiral core) with a diameter of 0.75 mm. The wave period is about 4 min.

Unpinning of spiral waves by electrical forcing is studied in a uniform thin layer of the BZ reaction using a flat reactor constructed from transparent Plexiglas [27]. The volume is  $100 \times 100 \times 1.0 \text{ mm}^3$ . An electric field is applied via two electrodes in electrolytic compartments (size of each 25  $\times$  $100 \times 2.0 \text{ mm}^3$ ), which are attached to the left and the right boundaries of the main volume [14]. Application of the electric field also results in gas bubbles formed by electrolysis. The bubbles cause the resistance between the electrodes to fluctuate in time. To specify precisely the strength of forcing, electricity driven by a power supply in a constant electrical current mode is utilized, and the strength of applied electrical forcing in the experiments is recorded as electrical current density instead of electric field, which is normally used in simulations. As an obstacle, a chemically inert plastic cylinder with a diameter of 0.4-1.5 mm and a height of 1.0 mm is attached in the main volume by using silicone paste before the BZ solution is filled into the reactor. During the experiments, the reactor is placed in a transparent thermostating bath to remove Ohmic heat and to set the temperature at 24 °C  $\pm$  1 °C. The bath is put between a white light source and a color CCD camera (Super-HAD, Sony) to record the images of the medium every second with a resolution of  $0.05 \text{ mm pixel}^{-1}$ .

A spiral wave pinned to the obstacle is initiated by the following procedure: The reactor is oriented vertically, and a volume of BZ solution is filled into the reactor, forming the first layer of 2.5 cm height, where the obstacle is located. Then, we wait until the gel is formed. Wave fronts are initiated by immersion of a silver wire of 0.5 mm diameter between the left edge of the reactor and the obstacle. One open end of the wave front propagates towards the obstacle [Fig. 1(a)], while the other moves close to the left edge of the reactor. Another volume of the BZ solution is added to the reactor as the second layer when the open end reaches the obstacle [Fig. 1(b)]. The final height of the medium is about 4.5–5.0 cm. Shortly after filling in the second layer, the open end of the wave front starts to curl in [Fig. 1(c)] to form a spiral wave with its tip rotating around the obstacle [Fig. 1(d)].

#### B. Results and discussion

Figure 1 shows the development of a pinned spiral wave in our experiments. As reported earlier [27,30,31], the atmospheric oxygen suppresses the excitability of a thin sheet below the top surface of the first layer [dark orange (dark gray) band in Figs. 1(a)-1(c)], so that the wave front does not reach the atmospheric interface. After the second layer is filled, this inhibited layer disappears when the dissolved oxygen is consumed during the first passage of the excitation front [see Fig. 1(c)]. We note that filling in the BZ solution to form the second layer must be done at the proper time, i.e., when the front reaches the obstacle, as depicted in Fig. 1(b). If this is done too early or too late (i.e., when the front does not touch the obstacle), the spiral wave will not be pinned.

For obstacles larger than the free spiral core, the tips of pinned spiral waves are always attached to the obstacle [as in

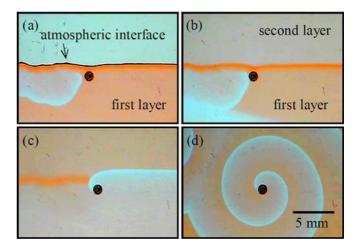


FIG. 1. (Color online) Pinning a spiral wave in the BZ reaction.

(a) A wave front is initiated by a silver wire in the first layer. (b) A portion of the BZ reaction is placed on top as the second layer, when the blue (light gray) front end reaches the obstacle (black circle; diameter of 1.05 mm). (c) The inhibited layer [dark orange (dark gray) band] disappears after the first passage of the wave front. (d) After three spiral rotations, the front adopts a typical spiral structure with its tip attached to the obstacle.

Fig. 1(d)]. In contrast, we observe alternations of attachment [Figs. 2(a) and 2(b)] and detachment [Figs. 2(c) and 2(d)] of the spiral tip in the vicinity of obstacles smaller than the free spiral core. The spiral core is an area in the refractory state, thus no wave can propagate into it. When a small obstacle occupies some part of the spiral core, the other (unoccupied) part is still in the refractory state and prohibits any wave propagation. As in Figs. 2(c) and 2(d), the spiral tip is temporarily detached from the obstacle, when it reaches such a refractory area. However, the free tip moves towards the obstacle again.

To investigate unpinning phenomena, we apply a constant current density J, which is stepwise increased from small to large values. For each value of the obstacle diameter, the

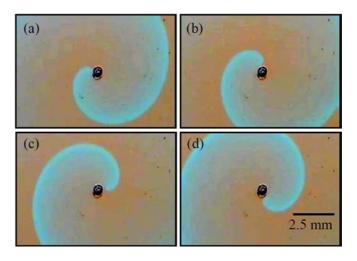


FIG. 2. (Color online) Motion of a spiral wave around a small obstacle in the BZ reaction. For each rotation, the spiral tip is alternately (a) and (b) attached to and (c) and (d) detached from the obstacle with a diameter of 0.4 mm.

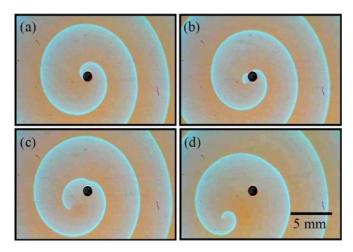


FIG. 3. (Color online) Unpinning of a spiral wave by electrical forcing in the BZ reaction. The obstacle diameter is 1.05 mm. The positive and negative electrodes are placed on the left- and the right-hand sides, respectively. (a) An electrical current density J=96 mA cm<sup>-2</sup> induces an anisotropic spiral structure with its tip still attached to the obstacle. When J reaches a critical value  $J_{\rm unpin}=98$  mA cm<sup>-2</sup>, (b) the spiral tip is detached and (c) and (d) subsequently moves away from the obstacle.

experiments are performed twice with different steps  $\Delta J = 10$  and 2 mA cm<sup>-2</sup>, respectively. In all experiments, each value of J is applied for an interval of three to five spiral rotations before J is increased. The spiral tip leaves the obstacle and moves away when J reaches a critical value  $J_{\rm unpin}$ , i.e., the minimal current density for unpinning. For guidance, the first experiment with the large step  $\Delta J = 10$  mA cm<sup>-2</sup> provides a rough estimate of electrical current density necessary for unpinning the spiral wave. The fine-tuning of J is obtained in the second experiment with  $\Delta J = 2$  mA cm<sup>-2</sup>. This way, one can obtain the finest value of  $J_{\rm unpin}$  ( $\Delta J = 2$  mA cm<sup>-2</sup>) available from our equipment within a relatively short observation time of up to 2 h, while the aging of the BZ reaction, which potentially affects the dynamics of the spiral wave in long running experiments, can be minimized.

Figure 3 demonstrates the unpinning phenomenon. With  $J < J_{\text{unpin}}$ , the spiral tip still remains attached to the obstacle. However, the forcing induces an anisotropically distorted spiral wave [see Fig. 3(a)] because the electrical current accelerates or decelerates the front propagating towards or away from the positive electrode [26], while the spiral tip remains pinned. For  $J \ge J_{\text{unpin}}$ , the spiral tip is detached from the obstacle [see Fig. 3(b)]. When the electrical current is continuously applied, the unpinned spiral tip moves towards the positive electrode with an angle. The anisotropic structure also changes with time [see Figs. 3(b)–3(d)]. As the spiral tip moves far away from the obstacle [Fig. 3(d)], we observed the deformed wave structure similar to a drifting spiral wave under electrical forcing in the absence of obstacles [24].

The necessary current density  $J_{\rm unpin}$  for unpinning the spiral wave increases with the obstacle diameter d, as shown in Fig. 4. For obstacles smaller than the free spiral core (d < 0.75 mm),  $J_{\rm unpin}$  increases with d, but the increase is slower than that for larger obstacles (d > 0.75 mm). To investigate the growth rate  $\Delta J_{\rm unpin}/\Delta d$ , we apply linear fits for the two ranges of the

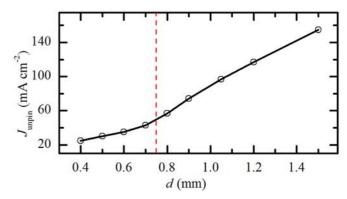


FIG. 4. (Color online) Electrical current density  $J_{\rm unpin}$  necessary for releasing a spiral wave pinned to an unexcitable obstacle with diameter d. The vertical dashed line at 0.75 mm indicates the core diameter of a free spiral wave.

obstacle diameter and find that  $\Delta J_{\rm unpin}/\Delta d=0.590\pm0.052$  and  $1.389\pm0.048~{\rm A~cm^{-3}}$  for  $d<0.75~{\rm mm}$  and  $d>0.75~{\rm mm}$ , respectively. Clearly,  $J_{\rm unpin}$  grows at a much higher rate for the large obstacles in comparison with that for the small ones. The results show that it is more difficult to release spiral waves pinned to larger obstacles, especially when the obstacle size exceeds that of the free spiral core.

#### III. SIMULATIONS

#### A. Methods

In our numerical simulations, we use the two-variable Oregonator model to describe the dynamics of the activator u and the inhibitor v (corresponding to the concentrations of HBrO<sub>2</sub> and the catalyst, respectively) in the BZ reaction. The advection terms for both u and v account for the electric field E applied in the x direction:

$$\frac{\partial u}{\partial t} = \frac{1}{\varepsilon} \left( u - u^2 - f v \frac{u - q}{u + q} \right) + D_u \nabla^2 u - M_u E \frac{\partial u}{\partial x},$$

$$\frac{\partial v}{\partial t} = u - v + D_v \nabla^2 v - M_v E \frac{\partial v}{\partial x}.$$
(1)

As in Refs. [14,29], the parameters are chosen as  $\varepsilon = 0.01$ , q = 0.002, f = 1.4, the diffusion coefficients  $D_u = 1.0$  and  $D_v = 0.6$ , and the ionic mobilities  $M_u = -1.0$  and  $M_v = 2.0$ . In the absence of an electric field, the tip of a free spiral wave rotates around a circular core [diameter = 0.9 system unit (s.u.)]. The spiral tip is defined as the intersection of the contour u = 0.15 and v = 0.0935 to ensure  $\partial u/\partial t = 0$  on the position of the tip [14].

The simulations are performed using an explicit Euler method with a nine-point approximation of the two-dimensional Laplacian operator and a centered-space approximation of the gradient term. The uniform grid space  $\Delta x = \Delta y = 0.025$  s.u. and the time step  $\Delta t = 1.9 \times 10^{-4}$  time unit (t.u.) are chosen as required for numerical stability  $[\Delta t \le (3/8)(\Delta x)^2 \ [32]]$ . The dimensionless size of the system is  $20 \times 20$  s.u. (corresponding to  $800 \times 800$  grid points). A completely unexcitable circular area is put as the obstacle. Therefore, the boundaries of both the medium and the obstacle have no-flux conditions.

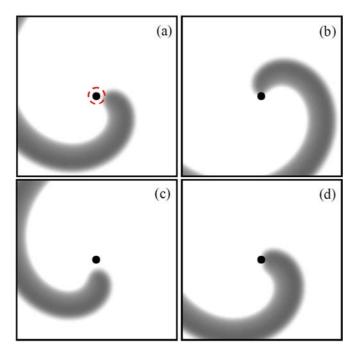


FIG. 5. (Color online) Motion of a spiral wave around a small obstacle in the Oregonator model. (a) At the beginning, an obstacle 0.5 s.u. in diameter is put in the middle of the spiral core (the dashed circle). (b) The tip moves towards and is attached to the obstacle. (c) Subsequently, it is detached from the obstacle, but (d) it is attached to the obstacle again.

To create a spiral wave, a planar wave is triggered by setting a five-grid-point strip at an edge of the medium to an excited state (e.g., u = 1.0 and v = 0 for  $0.0 \le x \le 0.5$ ). The wave front is allowed to propagate into the middle of the medium before half of the medium is reset to an excitable state (e.g., u = 0 and v = 0 for  $0.0 \le v \le 10.0$ ), leading to a free-end

wave front, which subsequently curls to form a rotating spiral wave. The circular obstacle (diameter d of 0.2–1.9 s.u.) is put in the middle of the spiral core after the spiral wave is allowed to propagate freely for several rotations.

#### B. Results and discussion

The obstacles affect the movement of the spiral tip in the same ways as found in our experiments. In the case of large obstacles, the spiral tip is simply attached to the obstacle at all times. However, alternations of attachment and detachment of the spiral tip to the obstacle smaller than the free spiral core are observed. Figure 5 illustrates the dynamics of the spiral tip in the vicinity of such a small obstacle with d=0.5 s.u. Shortly after the obstacle is put into the spiral core [see Fig. 5(a)], the spiral tip leaves its circular path (the dashed circle) and moves closer to the obstacle until getting attached to it [Fig. 5(b)]. Subsequently, the spiral tip is detached from the obstacle and moves away for a short distance [Fig. 5(c)] before moving back and being attached to the obstacle again [Fig. 5(d)].

As in our experimental results, the pinned spiral wave in the simulations is forced to drift away from the obstacle only when the applied electric field E reaches the critical value  $E_{\rm unpin}$  (the electric field necessary for unpinning). Figure 6 demonstrates the dynamics of a pinned spiral wave under the applied field. When E=0.625, which is very close to but weaker than  $E_{\rm unpin}$ , the spiral tip is alternately detached from [Figs. 6(a), 6(b), and 6(d)] and attached to [Figs. 6(c) and 6(e)] the obstacle.

The unpinning is successful at a slightly stronger field E = 0.630. At the beginning, the motion of the spiral tip seems similar to that at the weaker field [compare Figs. 6(a) and 6(b) with 6(a') and 6(b')]. On collision with the obstacle in Figs. 6(b) and 6(b'), a part of the front end (indicated by the arrows) is separated from the spiral wave. For E = 0.625, this small segment of the broken front end contracts until it

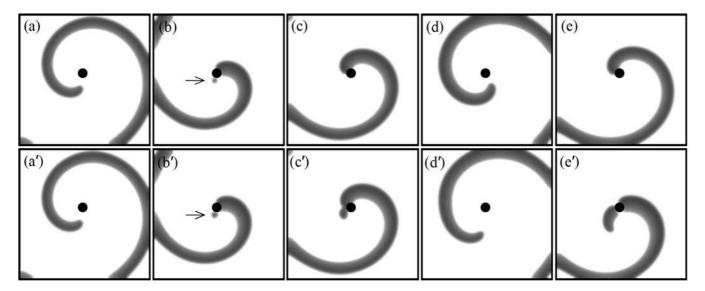


FIG. 6. Effect of an electrical field on a pinned spiral wave in the Oregonator model. The obstacle diameter is 1.5 s.u. The direction of the electric field E is pointing to the right of the images. (a)–(e) Forced temporary detachments: The spiral tip is alternately attached to and detached from the obstacle under E = 0.625. (a')–(e') Unpinning: The spiral tip is detached and moves away from the obstacle under E = 0.630. The arrows indicate the segments of broken front end.

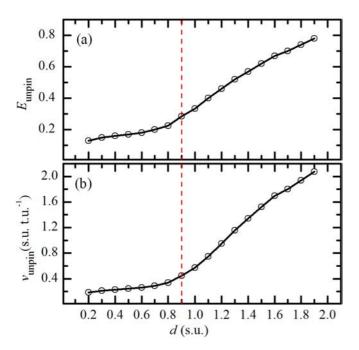


FIG. 7. (Color online) Necessary forcing to release a spiral wave pinned to an unexcitable obstacle with diameter d in the Oregonator model: (a) the electrical field  $E_{\rm unpin}$  and (b) the corresponding drift velocity  $v_{\rm unpin}$ . The vertical dashed line at 0.9 s.u. indicates the core diameter of a free spiral wave.

disappears, so that the spiral wave is attached to the obstacle again [Fig. 6(c)]. In contrast, this segment grows at E=0.630 and subsequently merges to the spiral structure, so that the spiral tip does not touch the obstacle [Fig. 6(c')]. The spiral tip drifts farther away from the obstacle over the course of time [see Figs. 6(a')-6(e')]; that is, the spiral wave is successfully unpinned from the obstacle.

The simulations not only reproduce the forced unpinning in our experiments but also reveal the forced temporary detachments around large obstacles [e.g., Figs. 6(a)–6(e)], which are not observed in the BZ reaction. We conjecture that the finest step of the electrical current density ( $\Delta J = 2$  mA cm<sup>-2</sup>) might be insufficiently small to allow these phenomena to occur in our experiments.

Figure 7(a) depicts the necessary applied field  $E_{\rm unpin}$  to unpin the spiral wave for different obstacle diameters d. Linear fits provide an approximation of the growth rate  $\Delta E_{\rm unpin}/\Delta d=0.145\pm0.011$  and  $0.501\pm0.016$  s.u.  $^{-1}$  for d<0.9 s.u. and d>0.9 s.u. This increment of  $E_{\rm unpin}$  with a much higher rate for obstacles larger than the free spiral core agrees well with the experiments (Fig. 4). To generalize the forcing, we performed additional simulations by applying the electric field  $E_{\rm unpin}$  [the same values as in Fig. 7(a)] to a free spiral wave (without obstacle) and measured the corresponding drift velocity ( $v_{\rm unpin}$ ) of the spiral tip. As shown in Fig. 7(b), the

dependence of  $v_{\rm unpin}$  on the obstacle size is similar to that of  $E_{\rm unpin}$ : the growth rate  $\Delta v_{\rm unpin}/\Delta d=0.227\pm0.022$  and  $1.69\pm0.045~{\rm s.u.}^{-1}$  for  $d<0.9~{\rm s.u.}$  and  $d>0.9~{\rm s.u.}$ 

The systematic studies in both experiments (Fig. 4) and simulations (Fig. 7) show that unpinning of spiral waves occurs under relative small forcing, when the obstacles are smaller than the free spiral core. This may be because the spiral tip is not tightly attached to those small obstacles: Its temporary detachments occur when the tip reaches the refractory area (Figs. 2 and 5) even in the absence of external forcing. In contrast, the spiral tip always touches larger obstacles.

Our investigation shows that stronger electrical forcing is needed for unpinning a spiral wave from a larger unexcitable obstacle in chemical media. This requirement of sufficient electrical forcing is consistent with earlier studies on unpinning by an external wave train [11,23,33], where the unpinning is successful only when the frequency of the wave train is higher than the critical value, which increases with the obstacle size. Since the highest frequency of waves is limited by the refractory time of the excitable medium, such unpinning is impossible when the obstacle is very large [11,23]. For some conditions, the pinned spiral wave can be released by the wave train only when the obstacle is smaller than the free spiral core [33]. It is demonstrated [33–35] that the situations can be improved by reducing the excitability of the medium, which leads to an enlargement of the spiral core size.

#### IV. CONCLUSIONS

We have presented an investigation of the release of a pinned spiral wave in the BZ reaction by electrical forcing. Under a small electrical current density, the spiral wave still remains pinned to an unexcitable cylindrical obstacle. When the electrical current density reaches a critical threshold, the spiral wave is released. The critical current density increases linearly stepwise with the diameter of the obstacle: it grows at a much higher rate for obstacles larger than the free spiral core in comparison to that of smaller obstacles. The experimental results are confirmed by simulations using the Oregonator model. From both parts of this study, we conclude that a release of a pinned spiral wave by an electric forcing is feasible for obstacle sizes both smaller and larger than the free spiral core. However, the study of such electrically forced unpinning becomes a tough endeavor when the wave is pinned to an obstacle larger than the free spiral core.

#### ACKNOWLEDGMENTS

We thank the Faculty of Science, the Research and Development Institute (KURDI), the Center for Advanced Studies of Industrial Technology, and the Graduate School, Kasetsart University; the German Academic Exchange Service (DAAD); and the Thailand Research Fund (Grant No. TRG5680044) for financial support.

S. Nettesheim, A. von Oertzen, H. H. Rotermund, and G. Ertl, J. Chem. Phys. 98, 9977 (1993).

<sup>[2]</sup> F. Siegert and C. J. Weijer, J. Cell Sci. 93, 325 (1989).

<sup>[3]</sup> J. M. Davidenko, A. M. Pertsov, R. Salomonz, W. Baxter, and J. Jalife, Nature (London) 355, 349 (1992).

<sup>[4]</sup> A. T. Winfree, Science 175, 634 (1972).

<sup>[5]</sup> A. T. Winfree, Science 181, 937 (1973).

<sup>[6]</sup> A. T. Winfree, Science 266, 1003 (1994).

<sup>[7]</sup> E. M. Cherry and F. H. Fenton, New J. Phys. 10, 125016 (2008).

- [8] A. P. Muñuzuri, V. Pérez-Muñuzuri, and V. Pérez-Villar, Phys. Rev. E 58, R2689 (1998).
- [9] C. W. Zemlin and A. M. Pertsov, Phys. Rev. Lett. 109, 038303 (2012).
- [10] J. P. Keener and J. J. Tyson, Physica D (Amsterdam, Neth.) 21, 307 (1986).
- [11] Y.-Q. Fu, H. Zhang, Z. Cao, B. Zheng, and G. Hu, Phys. Rev. E 72, 046206 (2005).
- [12] O. Steinbock and S. C. Müller, Physica A (Amsterdam, Neth.) 188, 61 (1992).
- [13] K. I. Agladze, R. A. Kocharyan, and V. I. Krinsky, Physica D (Amsterdam, Neth.) 49, 1 (1991).
- [14] C. Luengviriya, S. C. Müller, and M. J. B. Hauser, Phys. Rev. E 77, 015201 (2008).
- [15] Z. Jiménez, B. Marts, and O. Steinbock, Phys. Rev. Lett. 102, 244101 (2009).
- [16] Z. Jiménez and O. Steinbock, Europhys. Lett. 91, 50002 (2010).
- [17] I. R. Efimov, Y. N. Cheng, M. Biermann, D. R. Van Wagoner, T. Mazgalev, and P. J. Tchou, J. Cardiovasc. Electrophysiol. 8, 1031 (1997).
- [18] C. M. Ripplinger, V. I. Krinsky, V. P. Nikolski, and I. R. Efimov, Am. J. Physiol. Heart Circ. Physiol. 291, 184 (2006).
- [19] J. Cysyk and L. Tung, Biophys. J. 94, 1533 (2008).
- [20] M. Hörning, A. Isomura, K. Agladze, and K. Yoshikawa, Phys. Rev. E 79, 026218 (2009).
- [21] K. Agladze, M. W. Kay, V. Krinsky, and N. Sarvazyan, Am. J. Physiol. Heart Circ. Physiol. 293, 503 (2007).

- [22] A. Isomura, M. Hörning, K. Agladze, and K. Yoshikawa, Phys. Rev. E 78, 066216 (2008).
- [23] M. Tanaka, A. Isomura, M. Hörning, H. Kitahata, K. Agladze, and K. Yoshikawa, Chaos 19, 043114 (2009).
- [24] O. Steinbock, J. Schütze, and S. C. Müller, Phys. Rev. Lett. **68**, 248 (1992).
- [25] K. I. Agladze and P. De Kepper, J. Phys. Chem. **96**, 5239 (1992).
- [26] A. P. Muñuzuri, V. A. Davydov, V. Pérez-Muñuzuri, M. Gómez-Gesteira, and V. Pérez-Villar, Chaos Solitons Fractals 7, 585 (1996).
- [27] C. Luengviriya, U. Storb, M. J. B. Hauser, and S. C. Müller, Phys. Chem. Chem. Phys. 8, 1425 (2006).
- [28] R. J. Field and R. M. Noyes, J. Chem. Phys. **60**, 1877 (1974).
- [29] W. Jahnke and A. T. Winfree, Int. J. Bifurcation Chaos Appl. Sci. Eng. 1, 445 (1991).
- [30] A. F. Taylor, B. R. Johnson, and S. K. Scott, J. Chem. Soc. Faraday Trans. 94, 1029 (1998).
- [31] A. F. Taylor, B. R. Johnson, and S. K. Scott, Phys. Chem. Chem. Phys. 1, 807 (1999).
- [32] M. Dowle, R. M. Mantel, and D. Barkley, Int. J. Bifurcation Chaos Appl. Sci. Eng. **7**, 2529 (1997).
- [33] A. Pumir, S. Sinha, S. Sridhar, M. Argentina, M. Hörning, S. Filippi, C. Cherubini, S. Luther, and V. Krinsky, Phys. Rev. E 81, 010901(R) (2010).
- [34] Z. Y. Lim, B. Maskara, F. Aguel, R. Emokpae, and L. Tung, Circulation. 114, 2113 (2006).
- [35] C. Cabo, A. M. Pertsov, J. M. Davidenko, W. T. Baxter, R. A. Gray, and J. Jalife, Biophys. J. 70, 1105 (1996).

#### PHYSICAL REVIEW E 91, 052912 (2015)

#### Propagation of spiral waves pinned to circular and rectangular obstacles

Malee Sutthiopad, <sup>1</sup> Jiraporn Luengviriya, <sup>2,3</sup> Porramain Porjai, <sup>1</sup> Metinee Phantu, <sup>1</sup> Jarin Kanchanawarin, <sup>3</sup> Stefan C. Müller, <sup>4</sup> and Chaiya Luengviriya<sup>1,\*</sup>

<sup>1</sup>Department of Physics, Kasetsart University, 50 Phaholyothin Road, Jatujak, Bangkok 10900, Thailand <sup>2</sup>Department of Industrial Physics and Medical Instrumentation, King Mongkut's University of Technology North Bangkok, 1518 Pibulsongkram Road, Bangkok 10800, Thailand

<sup>3</sup>Lasers and Optics Research Group, King Mongkut's University of Technology North Bangkok, 1518 Pibulsongkram Road, Bangkok 10800, Thailand

<sup>4</sup>Institute of Experimental Physics, Otto-von-Guericke University Magdeburg, Universitätsplatz 2, D-39106 Magdeburg, Germany (Received 5 March 2015; published 15 May 2015)

We present an investigation of spiral waves pinned to circular and rectangular obstacles with different circumferences in both thin layers of the Belousov-Zhabotinsky reaction and numerical simulations with the Oregonator model. For circular objects, the area always increases with the circumference. In contrast, we varied the circumference of rectangles with equal areas by adjusting their width w and height h. For both obstacle forms, the propagating parameters (i.e., wavelength, wave period, and velocity of pinned spiral waves) increase with the circumference, regardless of the obstacle area. Despite these common features of the parameters, the forms of pinned spiral waves depend on the obstacle shapes. The structures of spiral waves pinned to circles as well as rectangles with the ratio  $w/h \sim 1$  are similar to Archimedean spirals. When w/h increases, deformations of the spiral shapes are observed. For extremely thin rectangles with  $w/h \gg 1$ , these shapes can be constructed by employing semicircles with different radii which relate to the obstacle width and the core diameter of free spirals.

DOI: 10.1103/PhysRevE.91.052912 PACS number(s): 05.45.—a, 05.65.+b, 82.40.Ck, 82.40.Qt

#### I. INTRODUCTION

Propagating spiral waves have been discovered in various reaction-diffusion systems such as CO oxidation on platinum surfaces [1], cell aggregation in slime mold colonies [2], electrical wave propagation in cardiac tissues [3], and concentration waves in the Belousov-Zhabotinsky (BZ) reaction [4,5]. In the heart, electrical spiral waves are connected with cardiac tachycardia and life-threatening fibrillations [6,7]. Such spiral waves may cease when their tip hits the boundary of the medium. However, they will survive much longer if they are pinned to anatomical inhomogeneities or obstacles, e.g., veins or scars [3].

Unexcitable disks have been widely taken as model obstacles to study the effects of obstacle size on the properties of spiral waves pinned to them. Tyson and Keener's theoretical work [8] predicted that a spiral wave rotating around a circular hole has period and velocity that increase when the hole is enlarged. Tanaka et al. [9] proposed a formula which showed that the spiral wave velocity at the periphery of the circular obstacle increases with the obstacle radius. Simulations by Fu et al. [10] revealed that both unexcitable and partially excitable circles cause the period of spiral waves to increase with their radii. Similarly, Cherubini et al. [11] showed that the wavelength and the period also increase linearly with the obstacle radius in cardiac model systems, regardless of whether the elasticity of the medium was included in the simulations. For spiral waves in cardiomyocytes, their velocity and wavelength were found to increase linearly with the circumference of the circular obstacle [12].

Experiments using thin layers of the photosensitive ruthenium-catalyzed BZ reaction [13] have demonstrated that

wave period, wavelength, and velocity of a spiral wave increased from 26 s, 1.3 mm, and 49.6  $\mu$ m s<sup>-1</sup> to 49 s, 3.4 mm, and 74.3  $\mu$ m s<sup>-1</sup>, respectively, after an artificial circular core was created by a laser spot of 1.2 mm in diameter. A scroll ring (i.e., a spiral structure in three dimensions) has been often observed to contract and eventually self-annihilate [14,15]. However, the contraction was suppressed when the scroll ring was pinned to spherical plastic beads [16,17].

In this article, we present an investigation of the dynamics of pinned spiral waves in BZ media. We chose two different simple forms of obstacles: circles and rectangles. Circles are symmetric objects which were used in many studies of pinned spiral waves in experiments and simulations, whereas rectangles have the advantage that their width and height are adjustable to obtain different circumferences while the area can be fixed to a constant value. We confirmed our experimental results by numerical simulations using the Oregonator model [18,19].

#### II. EXPERIMENTS

#### A. Experimental methods

We prepared the Belousov-Zhabotinsky (BZ) solutions from NaBrO<sub>3</sub>, H<sub>2</sub>SO<sub>4</sub>, malonic acid (MA), and ferroin, all purchased from Merck. Stock solutions of NaBrO<sub>3</sub> (1 M) and MA (1 M) were freshly produced by dissolving powder in deionized water (conductivity  $\sim 0.056~\mu S~cm^{-1}$ ), whereas stock solutions of H<sub>2</sub>SO<sub>4</sub> (2.5 M) and ferroin (25 mM) were commercially available. To prevent any hydrodynamic perturbation, the reaction was embedded in a 1.0% w/w agarose gel (Sigma). Appropriate volumes of the stock solutions were mixed and diluted in deionized water to form BZ solutions with initial concentrations: [H<sub>2</sub>SO<sub>4</sub>] = 160 mM,

<sup>\*</sup>Corresponding author: fscicyl@ku.ac.th

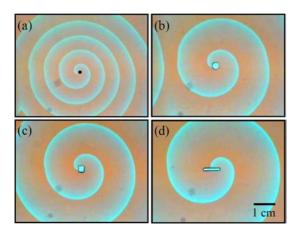


FIG. 1. (Color online) Spiral waves in the BZ reaction: (a) A free spiral wave (no obstacle) with a spiral core of 1.0 mm diameter (black circle), and spiral waves pinned to (b) a circle with diameter 2.8 mm and to rectangles with dimensions (c) 2.3 mm  $\times$  2.6 mm and (d) 6.5 mm  $\times$  0.9 mm.

[MA] = 50 mM, [NaBrO<sub>3</sub>] = 50 mM, and [ferroin] = 0.625 mM. At a temperature of 15 °C, the BZ solutions supported spiral waves with wavelength, period, and velocity of 7.5 mm,  $11.4 \, \text{min}$ , and  $0.66 \, \text{mm min}^{-1}$ , respectively.

The influence of unexcitable obstacles on the propagation of spiral waves (shown, e.g., in Fig. 1) was investigated in a uniform thin layer of the BZ reaction using a flat reactor (volume  $100 \times 100 \times 1.0 \text{ mm}^3$ ) constructed from transparent Plexiglas [20]. Eight circles with different diameters of 1.5, 1.9, 2.5, 2.8, 3.1, 3.5, 3.9, and 4.5 mm and four rectangles with width and height of  $2.3 \times 2.6$ ,  $4.6 \times 1.3$ ,  $4.9 \times 1.2$ , and  $6.5 \times 0.9 \text{ mm}^2$  were created also from Plexiglas plates (thickness 1.0 mm, the same as for the BZ layers) using a computerized laser cutting machine [see Figs. 1(b)–1(d) for examples of the obstacles]. The area A and the circumference l of circular and rectangular obstacles are summarized in Fig. 2(a). In each experiment, one obstacle was attached in the reactor before filling in the BZ solution.

A spiral wave pinned to an obstacle was initiated by a two-layer method as demonstrated earlier (cf. Fig. 1 in Ref. [21]). During the observations, the reactor was placed in a transparent thermostatting bath to control the temperature at  $15 \pm 0.1$  °C. The bath was set between a white light source and a color charge-coupled-device camera (Super-HAD, Sony) to record the images of the spiral wave every second with a resolution of 0.10 mm pixel<sup>-1</sup>. The wavelength, the period, and the velocity of spiral fronts were measured at locations at least one wavelength away from the tip of free spirals or from the obstacle edges to which the spirals were pinned to avoid the curvature effect as described in an earlier work [22].

It is worth noting that a difficulty of this experimental investigation comes from the long period of pinned spiral waves and emergences of undesired circular waves and free spirals that are often generated by some sources, like dust particles, in the BZ reaction. Due to their shorter period, these waves, especially the free spirals, interact and subsequently overcome the pinned spiral waves after some time, as mentioned earlier by Steinbock and Müller in Ref. [13]. If such undesired waves occur, by chance,

near the obstacles and the structure of pinned spiral wave is perturbed, the measurement criterion described above cannot be fulfilled. In this case, the experiments were repeated with new preparations of the BZ reaction. Therefore, carefully cleaning of the reactor as well as the obstacles before the experiments should be done to minimize the undesired waves.

#### **B.** Experimental results

Figure 1 illustrates examples of spiral waves with different wavelengths observed in our experiments. In the absence of obstacles, the BZ solutions supported spiral waves with wavelength  $\lambda=7.5$  mm and the spiral tip (measured location as in Ref. [20]) traced a circular area of 1.0 mm in diameter, as in Fig. 1(a). Spiral waves pinned to obstacles having a similar area of about 6 mm² but differing in shape and circumference l are shown in Figs. 1(b)–1(d). The wavelength  $\lambda$  was enlarged to 14.3 mm for the case of a circle with diameter 2.8 mm [l=8.8 mm, Fig. 1(b)]. A similar wavelength ( $\lambda=14.4$  mm) was observed for the rectangle with dimensions 2.3 mm  $\times$  2.6 mm [l=9.8 mm, Fig. 1(c)]. The longer rectangle with dimensions 6.5 mm  $\times$  0.9 mm [l=14.8 mm, Fig. 1(d)] resulted in a much larger wavelength of 20.3 mm.

Figure 2 summarizes the properties of pinned spiral waves as well as obstacles investigated in our experiments. Since free spiral waves in the BZ solutions rotated around a circular core with diameter of 1.0 mm, we considered the core as a circular obstacle and included the properties of the free spirals

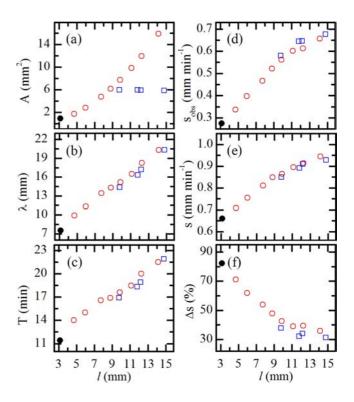


FIG. 2. (Color online) Properties of spiral waves as a function of the obstacle circumference l in the BZ reaction: (a) obstacle area A, (b) wavelength  $\lambda$ , (c) wave period T, [(d) and (e)] velocities  $s_{\rm obs}$  and s of waves adjacent to and far from the obstacles, respectively, and (f) percentage difference  $\Delta s$  between  $s_{\rm obs}$  and s. Filled circles: no physical obstacles (spiral core diameter 1.0 mm); open circles: circular obstacles; open rectangles: rectangular obstacles.

in Fig. 2 (see filled circles) for the purpose of comparison. Figure 2(a) shows the relation between area and circumference of the obstacles. As the diameter increases from 1.0 to 4.5 mm, the circumference l and the area A of the circles increase simultaneously from 3.1 to 14.1 mm and 0.8 to 15.9 mm², respectively. In contrast, the four rectangles  $(2.3 \times 2.6, 4.6 \times 1.3, 4.9 \times 1.2, \text{ and } 6.5 \times 0.9 \text{ mm}^2)$  with a circumference l ranging between 9.8 and 14.8 mm have almost the same area size of about 6 mm².

The spiral waves propagated around the obstacles with wavelength  $\lambda$  [Fig. 2(b)] and wave period T [Fig. 2(c)] increasing with the obstacle circumference l in both the cases of circles and rectangles. Moreover, data points from all obstacles lay approximately on the same line of each graph. The growth rate of the wavelength and the period with respect to the circumference are estimated by linear fits as  $\lambda/l = 1.064$  $\pm 0.043$  and  $T/l = 0.806 \pm 0.047$  min mm<sup>-1</sup>. To investigate the influence of the obstacles on the velocity of the spiral waves, we calculated the average velocity of the wave ends attached to the obstacles  $s_{obs}$  as the ratio between the circumference and the period  $s_{\text{obs}} = l/T$  as well as that of the spiral fronts far away from the obstacles s as the ratio between the wavelength and the period  $s = \lambda/T$ . As shown in Figs. 2(d) and 2(e), both  $s_{obs}$ and s increase with l. Even though  $s_{\rm obs}$  is always smaller than s for a given obstacle, its growth rate of  $s_{\rm obs}$  ( $s_{\rm obs}/l = 0.037 \pm$  $0.002 \, \mathrm{min}^{-1}$ ) is larger than that of  $s \, (s/l = 0.024 \pm 0.002)$  $\min^{-1}$ ). Therefore, their percentage difference [ $\Delta s(\%)$  =  $|s_{\rm obs} - s|/(s_{\rm obs} + s)/2 \times 100$ ] becomes smaller, while the circumference increases, as indicated in Fig. 2(f).

The structure of pinned spiral waves is also affected by the obstacles, as shown in Fig 3. During their evolution around circles, the spiral shape remains unchanged all the time and is well fitted by an Archimedean spiral [Fig. 3(a)]. For a rectangle with the width w similar to the height h (i.e., w/h = 0.9), the pinned spiral wave still looks similar to an Archimedean spiral [Fig. 3(b)]. When the ratio w/h of the rectangle is increased (i.e., to a more asymmetric shape), the spiral deviates farther from an Archimedean one [e.g., in Fig. 3(c) with w/h = 7.2]. In fact, the observed structures differ from any other mathematical spiral known to us (i.e., Euler's, Fermat's, hyperbolic, logarithmic spirals, etc.). These unusual spiral shapes also change periodically, while the waves rotate around the obstacles. As shown in Fig. 3(c),

the wave front near the obstacle has a high curvature when the wave end turns around the short boundaries on the left and the right. As the wave end propagates further along the long edges (the upper and the lower walls), the curvature of the nearby front continually decreases. A description of a spiral wave pinned to a rectangle similar to Fig. 3(c), but with extremely high w/h, is given in the section of simulation results (see Figs. 7 and 8).

#### III. SIMULATIONS

#### A. Simulation methods

Numerical simulations have been performed using the two-variable Oregonator model, as in Eq. (1), to describe the dynamics of the activator u and the controller v which account for the concentrations of HBrO<sub>2</sub> and the catalyst in the BZ reaction, respectively,

$$\frac{\partial u}{\partial t} = \frac{1}{\varepsilon} \left( u - u^2 - f v \frac{u - q}{u + q} \right) + D_u \nabla^2 u,$$

$$\frac{\partial v}{\partial t} = u - v + D_v \nabla^2 v.$$
(1)

As in a study by Jahnke and Winfree [19], the parameters were chosen as  $\varepsilon = 0.01$ , q = 0.002, f = 1.4, and the diffusion coefficients as  $D_u = 1.0$  and  $D_v = 0.6$ . For this parameter set, the system supported spiral waves with a circular spiral core of 0.9 space units (s.u.) in diameter, wavelength = 10.5 s.u., period = 1.55 time units (t.u.), and velocity = 6.76 s.u. t.u.<sup>-1</sup>.

The variables u and v in Eq. (1) were calculated using an explicit Euler method with a nine-point approximation of the two-dimensional Laplacian operator on a discrete system of a dimensionless size =  $160 \times 160$  s.u. with a uniform grid space of  $\Delta x = \Delta y = 0.1$  s.u. and a time step  $\Delta t = 3.0 \times 10^{-3}$  t.u., as required for numerical stability [ $\Delta t < (3/8)(\Delta x)$ ]<sup>2</sup> [23]). A single unexcitable circle or rectangle was defined as the obstacle in each simulation. The boundaries of both the medium and the obstacle had no-flux conditions. The implementation of a circular obstacle with no-flux boundary was described in a recent publication [24]. We tested totally 10 circles with different diameters of 1.5, 2.0, 3.0, 4.0, 5.0, 6.0, 7.0, 8.0, 9.0, and 10.0 s.u. and six rectangles with widths

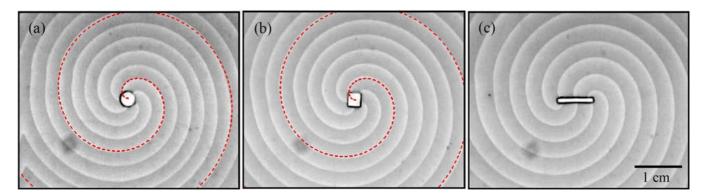


FIG. 3. (Color online) Image overlays of counterclockwise rotating spiral waves pinned to (a) a circle with diameter 2.8 mm and to rectangles with dimensions (b)  $2.3 \text{ mm} \times 2.6 \text{ mm}$  and (c)  $6.5 \text{ mm} \times 0.9 \text{ mm}$  in the BZ reaction. Dashed curves in (a) and (b) are Archimedean spirals with origins located at the obstacle centers.

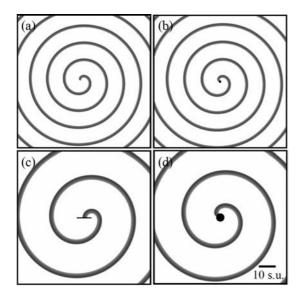


FIG. 4. Spiral waves in the Oregonator model: (a) a free spiral wave (no obstacle, spiral core diameter 0.9 s.u.) and spiral waves pinned to (b) a circle with diameter of 1.5 s.u., (c) a rectangle with dimensions  $8.5 \, \text{s.u.} \times 0.2 \, \text{s.u.}$  and (d) a circle with diameter of  $5.0 \, \text{s.u.}$ 

and heights of 1.3  $\times$  1.3, 1.7  $\times$  1.0, 3.4  $\times$  0.5, 5.4  $\times$  0.3, 8.5  $\times$  0.2, and 17.0  $\times$  0.1 s.u.<sup>2</sup>.

To create a spiral wave pinned to an obstacle, a planar wave was triggered by setting a five-grid-point strip at the left edge of the medium to an excited state (e.g., u=1.0 and v=0 for  $0.0 \leqslant x \leqslant 0.5$ ). When the wave front reached the obstacle (around the middle of the medium), half of the medium was reset to an excitable state (e.g., u=0 and v=0 for  $80.0 \leqslant y \leqslant 160.0$ ), leading to a planar wave with two ends attached to the edges of the obstacle and the system. Subsequently, the wave front curled to form a pinned spiral wave rotating around the obstacle (cf. Fig. 1 in Ref. [21]).

#### **B.** Simulation results

Examples of spiral waves with wavelengths depending on the obstacle circumference in the Oregonator model are shown in Fig. 4. A free spiral wave, as in Fig. 4(a), has a wavelength  $\lambda = 10.5$  s.u. and its tip rotates around a circular core (diameter 0.9 s.u.). Spiral waves pinned to three different obstacles are shown in Figs. 4(b)-4(d). A small circle with a diameter of 1.5 s.u. (area A = 1.77 s.u.<sup>2</sup>, circumference l = 4.7 s.u.), in Fig. 4(b), caused a small expansion of the wavelength to 10.7 s.u., while a rectangle with dimensions 8.5 s.u.  $\times$  0.2 s.u. with a smaller area  $A = 1.70 \text{ s.u.}^2$ , but a much longer l = 17.4 s.u., in Fig. 4(c), resulted in a spiral wave with a wavelength  $\lambda$  = 20.7 s.u. In Fig. 4(d), a pinned spiral wave with a wavelength  $\lambda = 20.2$  s.u., similar to that in Fig. 4(c), was obtained from a circular obstacle with a diameter of 5.0 s.u. having a similar circumference (l = 15.7 s.u.) but much larger area (A = 19.64 s.u.<sup>2</sup>) in comparison to the rectangle in Fig. 4(c).

The properties of pinned spiral waves and obstacles in our simulations are presented in Fig. 5. As in the experimental part, the free spiral waves were taken as if they were pinned to a circular obstacle with diameter of 0.9 s.u. and their properties

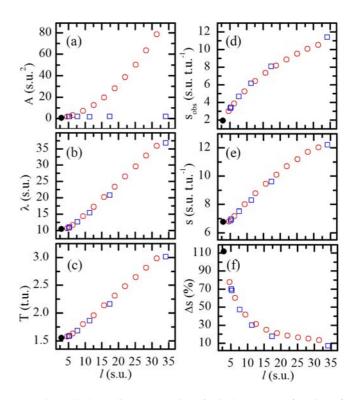


FIG. 5. (Color online) Properties of spiral waves as a function of the obstacle circumference l in the Oregonator model: (a) obstacle area A, (b) wavelength  $\lambda$ , (c) wave period T, [(d) and (e)] velocities  $s_{\rm obs}$  and s of waves adjacent to and far from the obstacles, respectively, and (f) percentage difference  $\Delta s$  of  $s_{\rm obs}$  and s. Filled circles: no physical obstacles (spiral core diameter 0.9 s.u.); open circles: circular obstacles; open rectangles: rectangular obstacles.

were included in this figure (see the filled circles). The obstacle areas A with different circumferences l are shown in Fig. 5(a). For the circular obstacles, the circumference l and the area A increase simultaneously from 3.0 to 31.4 s.u. and 0.71 to 78.55 s.u.<sup>2</sup>, respectively, when the diameter increases from 0.9 to 10.0 s.u. In contrast, the six rectangles with circumferences l between 5.2 and 34.2 s.u. have similar area sizes of 1.62-1.70 s.u.<sup>2</sup>. As shown in Figs. 5(b)-5(f), both circular and rectangular obstacles affected the properties of simulated spiral waves in the same manner as found in the experiments. The wavelength  $\lambda$  and the period T increase monotonously with a growth rate of  $\lambda/l = 0.921 \pm 0.020$  and  $T/l = 0.052 \pm$ 0.001 t.u. s.u.<sup>-1</sup>. For a given obstacle, the waves adjacent to the obstacle always propagate slower than the waves far from the obstacle ( $s_{\rm obs} < s$ ) but the rate  $s_{\rm obs}/l = 0.288 \pm 0.015$ t.u.<sup>-1</sup> is larger than  $s/l = 0.195 \pm 0.006$  t.u.<sup>-1</sup>. Thus, the percentage difference  $\Delta s$  of the velocities decreases, while the circumference increases.

Figure 6 illustrates examples of spiral structures for different obstacles. For circles and squares (i.e., the ratio of width and height w/h = 1.0), the shape of the spiral waves is approximated by Archimedean spirals, as in Figs. 6(a) and 6(b), respectively. For other rectangles with w/h > 1, the spiral waves adapt to unusual shapes, which change periodically as observed in our experiments. Figure 6(c) depicts a spiral wave rotating around a rectangle with extremely high w/h of 170. Shortly after the spiral performs a narrow U turn at the left and

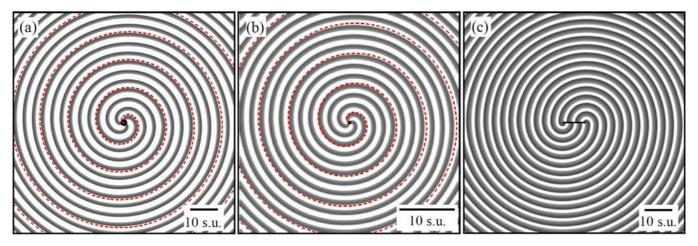


FIG. 6. (Color online) Image overlays of counterclockwise rotating spiral waves pinned to (a) a circle with diameter 5.0 s.u. mm and to rectangles with dimensions (b) 1.3 s.u.  $\times$  1.3 s.u. and (c) 17.0 s.u.  $\times$  0.1 s.u. in the Oregonator model. Dashed curves in (a) and (b) are Archimedean spirals with origins located at the obstacle centers.

the right ends, the wave front near the obstacle has a very high curvature. Then its curvature decreases, while the wave front traces the horizontal upper and lower walls of the obstacle.

In the following, we consider the spiral shapes in Fig. 6(c), as a first attempt to describe the structures of spiral waves pinned to rectangular obstacles. The overlaid image in Fig. 6(c) is separated into two sections: an upper and a lower half as shown in Figs. 7(a) and 7(b), respectively. Interestingly, they look like two halves of the well-known target patterns, which are often observed in excitable media. All wave fronts in both Figs. 7(a) and 7(b) fit to semicircles, the centers of which are close to (but do not touch) the right and the left boundary of the obstacle, respectively. Figures 7(c)-7(e) show a time series of the segment of a wave front close to the obstacle, while the spiral turns around the right boundary. When the segment reaches the lower right corner, it is almost planar and propagates to the right [Fig. 7(c)]. Shortly afterwards it passes the corner and an additional semicircular front appears [Fig. 7(d)]. Subsequently, the semicircular front expands above the obstacle, as if it is emitted from a point source according to the Huygens principle. The center of the point source is located at a distance  $\delta \sim 0.5$  s.u. away from the obstacle wall [Fig. 7(e)]. Note that the distance  $\delta$  is approximately half of the core diameter of a free spiral wave (0.9 s.u.).

Figure 8(a) illustrates a construction of the structure of the spiral wave with its end moving along the upper boundary of a very thin rectangle (dimensions =  $17.0 \text{ s.u.} \times 0.1 \text{ s.u.}$ ) by using the upper and lower semicircles shown in Figs. 7(a) and 7(b). Starting from the wave end attached to the obstacle, the wave front fits to the upper half of the smallest circle C<sub>0</sub>. Then it continues with the lower half of the next circle  $C_1$ . Subsequently, the front alternates to the upper half of the circle  $C_2$  and the lower half of the next circle  $C_3$ , respectively. In Fig. 8(b), centers and radii of the circles are drawn. The centers of C<sub>0</sub> and C<sub>2</sub> are located close to the right boundary of the obstacle, whereas those of  $C_1$  and  $C_3$  are at the left boundary. The centers are far from the boundary at the same distance ( $\delta \sim 0.5$  s.u.). This description is valid for a time interval of about half the rotation period, i.e., during the time that the wave end needs to trace the upper boundary of the obstacle from the right to the left end. Then the wave end turns at the left boundary and a new smallest semicircular wave (new  $C_0$ ) appears at the lower boundary. This spiral shape can

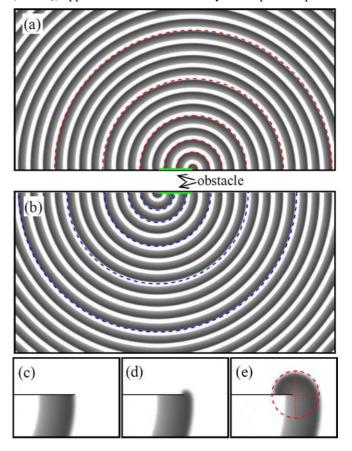


FIG. 7. (Color online) Estimation of the structure of a spiral wave pinned to a very thin rectangle in the Oregonator model. Some wave fronts in (a) the upper and (b) the lower sections of the overlaid image in Fig. 6(c) are compared to semicircles (dashed curves), the centers of which are located close to the right and the left edges of the obstacle. [(c)-(e)] When the wave front turns by an angle of  $180^{\circ}$  at the right boundary, a semicircular front appears, as if it is produced from a point source [the center of the dashed circle in (e)].

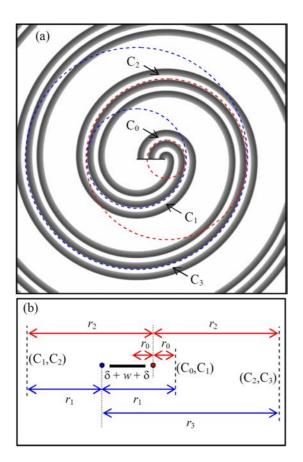


FIG. 8. (Color online) Graphical description of the structure of a spiral wave pinned to a very thin rectangle (black bar) using semicircles. (a) Three consecutive plots of the counterclockwise rotating spiral with the end tracing the upper boundary of the obstacle. The spiral structure at some instant of time can be estimated as a curve that alternately connects upper and lower semicircles of different sizes (corresponding halves of the dashed circles  $C_0$  to  $C_3$ ). (b) Estimation of the radii  $r_0$  to  $r_3$  of the circles  $C_0$  to  $C_3$  having different centers (two small filled circles) close to the left and the right boundary of the obstacle. For the purpose of illustration, the distance  $\delta$  is enlarged to a scale different from that of the width w and the radii  $r_0$  to  $r_3$ . The vertical dashed lines represent the contact positions of semicircle pairs as indicated by the labels.

be described in the same manner after a reorganization of the circles  $C_0$  to  $C_3$  and their centers.

According to the lifetime of the smallest circle  $C_0$ , which is limited to about half of the rotation period as described above, the radius  $r_0$  of the growing  $C_0$  is also limited by the obstacle width w and the distance  $\delta$  of the circle center:  $0 < r_0 \le w + \delta$ . It can be clearly seen in Fig. 8(b) that the radii of the larger circles are related to  $r_0$ , w, and  $\delta$  as  $r_n = r_0 + n(w + 2\delta)$ , where n is an integer.

#### IV. DISCUSSION AND CONCLUSION

We have presented an investigation of spiral waves pinned to unexcitable obstacles with different sizes and shapes in thin layers of the BZ reaction as well as in simulated systems based on the Oregonator model. Circles with increasing areas and circumferences and rectangles with equal areas but different circumferences were chosen as the obstacles. The

results in Figs. 1, 2, 4, and 5 show the common features of the influence of these obstacles on the spiral waves: The pinned spirals propagate with their wavelength, period, and velocity increasing with the obstacle circumference, regardless of the obstacle area. This implies that for such pinning phenomena, the obstacle sizes are more influential due to their circumferences than by their areas.

The time and space units of the simulations are related to the experiments as t.u. =  $1/k_5[MA + BrMA]$  and s.u. =  $\sqrt{D/k_5[MA + BrMA]}$ , where the rate of reaction  $k_5$  and the diffusion D of HBrO<sub>2</sub> are  $0.4 \,\mathrm{M}^{-1}\mathrm{s}^{-1}$  and  $1.5 \times 10^{-5} \mathrm{cm}^2\mathrm{s}^{-1}$ , respectively (cf. Ref. [19]). We used [MA+BrMA] = 0.050 M in the experiments so t.u. = 0.83 min and s.u. = 0.27 mm, which results in the core diameter, wavelength, period, and velocity of the free spiral waves as 0.25 mm, 2.88 mm, 1.29 min, and 2.22 mm min<sup>-1</sup>, respectively. These calculations imply that the excitability in our simulations is relatively higher than that of the real BZ reaction in our experiments, since the simulated spirals had a smaller core diameter, shorter wavelength, shorter period, and higher velocity than for the case of BZ spiral waves. In addition, although our simulations were performed in the excitable regime of the local dynamics [19], we conjecture that pinned spiral waves in oscillatory media would behave in a similar manner. This would hold at least for cases of long period oscillations, because the oscillations will be suppressed by rotating spiral waves with shorter periods, as found in experiments reported earlier [13] as well as in this study.

Tyson and Keener described in Ref. [8] that in determining the angular frequency  $\omega$  and the asymptotic normal velocity c (at locations far from the hole) of a spiral wave rotating around a hole with radius  $r_0$  in a given medium, the curvature relation ( $\omega$  as a function of c and  $r_0$ ) and the dispersion relation (c as a function of  $\omega$ ) must be simultaneously satisfied (see Eq. (24) in Ref. [8]). Both relations are nonlinear and can be solved graphically. Examples for various choices of  $r_0$  in the Oregonator model are given in Fig. 18 of Ref. [8] (a graph of the velocity c versus the period T). It is clear from the intersections of the curves that both the velocity c and the period T of the spiral wave increase simultaneously with the hole radius  $r_0$ . The results also imply that the wavelength  $\lambda$  increases with  $r_0$ , since  $\lambda = c$  T. Thus, our measurements of both circular and rectangular obstacles shown in Figs. 2, 5(b), 5(c), and 5(e) are consistent with the prediction in Ref. [8], even though it was derived only for the circular case. The necessity of the adjustment of the angular frequency  $\omega$  due to the presence of a circular hole in the core region of Archimedean spiral waves has been confirmed in a theoretical study by M. Tsoi [25]. Starting from the curvature effect and the methods employed in Ref. [8], Tanaka et al. [9] showed that the velocity of a spiral wave at the periphery of a circular obstacle increases with the radius of the obstacle (cf. Eq. (8) in Ref. [9]), which agrees well with our results in Figs. 2(d) and 5(d).

Our present findings show that the proposed theories in Refs. [8,9], which predict how the properties of a pinned spiral wave depend on the radius of a circular obstacle, are also valid for other forms (at least for rectangles) after introducing a small modification in the formulas, e.g., replacing the radius r of the circular obstacle by an equivalent quantity  $l/2\pi$  (since  $r = l/2\pi$  for a circle), where l is the obstacle circumference.

Circular obstacles have been used in many investigations of the influence of obstacle size on the release of pinned spiral waves. A train of electrical stimuli with a sufficiently high frequency  $f_{\text{unpin}}$  can induce unpinning of spiral waves. The  $f_{\text{unpin}}$  increases with the obstacle diameter [9,26–28]. An applied electric field causes reorientation and deformation of ring-shaped filaments of three-dimensional spiral waves (so-called scroll rings) that are pinned to a pair of unexcitable spheres in a BZ solution before the filaments are detached from these spheres [29]. A recent investigation [21] on the unpinning of spiral waves by an applied electrical current in the BZ reaction illustrated that a current with a density higher than a critical value  $J_{\text{unpin}}$  can release spiral waves pinned to circular unexcitable objects. Similarly to the frequency  $f_{\text{unpin}}$ , the  $J_{\text{unpin}}$  increases with the obstacle diameter. Further studies on the unpinning of spiral waves from obstacles with other forms, e.g., rectangles, are suggested to elucidate whether the critical value of the forcing (for instance, the frequency  $f_{\text{unpin}}$ of the wave train and the critical current density  $J_{\text{unpin}}$ ) relates solely to the obstacle circumference, as in the case for the properties of pinned spiral waves investigated here.

In contrast to the common features of the parameters of propagation in Figs. 2 and 5, the circular and rectangular obstacles result in different shapes of the spiral waves pinned to them. As shown in Figs. 3 and 6, the spirals are similar to Archimedean ones when pinned to circles or rectangles with a width w similar to the height h ( $w/h \approx 1$ ), while the ones pinned to asymmetric rectangles have unusual forms, which also change with time. The structure of a spiral wave pinned

to a rectangle with extremely high w/h can be described by using semicircles with radii depending on the width w and the core diameter (2 $\delta$ ) of free spirals, as illustrated in Figs. 7 and 8.

It has been shown earlier that the shapes of free spiral waves with circular cores [30] or those pinned to circular obstacles [31] are comparable to Archimedean spirals. Actually, meandering spiral waves rotating about noncircular cores [22 and references therein] have been more often observed, since they occur in broad ranges of system parameters of excitable media. The structures of these spirals, especially for extremely anisotropic cases like Z-shaped and linear cores [32-35], are complicated and have not yet been analyzed sufficiently. We assume that the structure of spiral waves pinned to a very thin rectangular obstacle, as described in this study, is similar to but simpler than that of free spiral waves with linear cores. While the thin rectangle remains at the same location all the time, the orientation of the linear cores is time dependent (see, e.g., Fig. 6(a) in Ref. [32] and Fig. 1(f) in Ref. [34]). Therefore, the fixed thin rectangular obstacle might be taken as a special case of the linear cores that remain stable or change very slowly in time.

#### ACKNOWLEDGMENTS

We thank the Department of Physics, the Faculty of Science, the Research and Development Institute (KURDI), the Center for Advanced Studies of Industrial Technology, the Graduate School, Kasetsart University, and the Thailand Research Fund (Grant No. TRG5680044) for financial support.

- S. Nettesheim, A. von Oertzen, H. H. Rotermund, and G. Ertl, J. Chem. Phys. 98, 9977 (1993).
- [2] F. Siegert and C. J. Weijer, J. Cell Sci 93, 325 (1989).
- [3] J. M. Davidenko, A. M. Pertsov, R. Salomonz, W. Baxter, and J. Jalife, Nature 335, 349 (1992).
- [4] A. T. Winfree, Science 175, 634 (1972).
- [5] J. Ross, S. C. Müller, and C. Vidal, Science 240, 460 (1988).
- [6] A. T. Winfree, Science 266, 1003 (1994).
- [7] E. M. Cherry and F. H. Fenton, New J. Phys. 10, 125016 (2008).
- [8] J. J. Tyson and J. P. Keener, Physica D 32, 327 (1988).
- [9] M. Tanaka, A. Isomura, M. Hörning, H. Kitahata, K. Agladze, and K. Yoshikawa, Chaos 19, 043114 (2009).
- [10] Y. Q. Fu, H. Zhang, Z. Cao, B. Zheng, and G. Hu, Phys. Rev. E 72, 046206 (2005).
- [11] C. Cherubini, S. Filippi, and A. Gizzi, Phys. Rev. E 85, 031915 (2012).
- [12] Z. Y. Lim, B. Maskara, F. Aguel, R. Emokpae, and L. Tung, Circulation 114, 2113 (2006).
- [13] O. Steinbock and S. C. Müller, Physica A 188, 61 (1992).
- [14] K. I. Agladze, R. A. Kocharyan, and V. I. Krinsky, Physica D 49, 1 (1991).
- [15] C. Luengviriya, S. C. Müller, and M. J. B. Hauser, Phys. Rev. E 77, 015201 (2008).
- [16] Z. A. Jiménez, B. Marts and O. Steinbock, Phys. Rev. Lett. 102, 244101 (2009).
- [17] Z. Jiménez and O. Steinbock, Europhys. Lett. **91**, 50002 (2010).

- [18] R. J. Field and R. M. Noyes, J. Chem. Phys. **60**, 1877 (1974).
- [19] W. Jahnke and A. T. Winfree, Int. J. Bif. Chaos 1, 445 (1991).
- [20] C. Luengviriya, U. Storb, M. J. B. Hauser, and S. C. Müller, Phys. Chem. Chem. Phys. 8, 1425 (2006).
- [21] M. Sutthiopad, J. Luengviriya, P. Porjai, B. Tomapatanaget, S. C. Müller, and C. Luengviriya, Phys. Rev. E **89**, 052902 (2014).
- [22] J. Luengviriya, P. Porjai, M. Phantu, M. Sutthiopad, B. Tomapatanaget, S. C. Müller, and C. Luengviriya. Chem. Phys. Lett. 588, 267 (2013).
- [23] M. Dowle, R. M. Mantel, and D. Barkley, Int. J. Bif. Chaos 7, 2529 (1997).
- [24] J. Luengviriya, M. Sutthiopad, M. Phantu, P. Porjai, J. Kanchanawarin, S. C. Müller, and C. Luengviriya. Phys. Rev. E **90**, 052919 (2014).
- [25] M. Tsoi, Persistence of planar spiral waves under domain truncation near the core, Ph.D. thesis, The Ohio State University, 2006.
- [26] K. Agladze, M. W. Kay, V. Krinsky, and N. Sarvazyan, Am. J. Physiol. Heart Circ. Physiol. 293, H503 (2007).
- [27] A. Isomura, M. Hörning, K. Agladze, and K. Yoshikawa, Phys. Rev. E 78, 066216 (2008).
- [28] A. Pumir, S. Sinha, S. Sridhar, M. Argentina, M. Hörning, S. Filippi, C. Cherubini, S. Luther, and V. Krinsky, Phys. Rev. E 81, 010901(R) (2010).
- [29] Z. A. Jiménez, Z. Zhang, and O. Steinbock, Phys. Rev. E 88, 052918 (2013).

- [30] S. C. Müller, Th. Plesser, and B. Hess, Physica D **24**, 87 (1987).
- [31] J. P. Keener and J. J. Tyson, Physica D **21**, 307 (1986).
- [32] V. I. Krinsky, I. R. Efimov, and J. Jalife, Proc. R. Soc. London Ser. A 437, 645 (1992).
- [33] M. A. Dahlem and S. C. Müller, Exp. Brain Res. 115, 319 (1997).
- [34] F. H. Fenton, E. M. Cherry, H. M. Hastings and S. J. Evans, Chaos 12, 852 (2002).
- [35] N. Manz, B. T. Ginn, and O. Steinbock, J. Phys. Chem. A 107, 11008 (2003).

#### Unpinning of spiral waves by electrical forcing in excitable chemical media

Malee Sutthiopad, <sup>1</sup> Jiraporn Luengviriya, <sup>2,3</sup> Porramain Porjai, <sup>1</sup> Boosayarat Tomapatanaget, <sup>4</sup> Stefan C. Müller, <sup>5</sup> and Chaiya Luengviriya<sup>1,\*</sup>

<sup>1</sup>Department of Physics, Kasetsart University, 50 Phaholyothin Road, Jatujak, Bangkok 10900, Thailand <sup>2</sup>Department of Industrial Physics and Medical Instrumentation, King Mongkut's University of Technology North Bangkok, 1518 Pibulsongkram Road, Bangkok 10800, Thailand

<sup>3</sup>Lasers and Optics Research Group, King Mongkut's University of Technology North Bangkok, 1518 Pibulsongkram Road, Bangkok 10800, Thailand

<sup>4</sup>Department of Chemistry, Chulalongkorn University, Bangkok 10330, Thailand
<sup>5</sup>Institute of Experimental Physics, Otto-von-Guericke University Magdeburg, Universitätsplatz 2, D-39106 Magdeburg, Germany (Received 12 February 2014; published 8 May 2014)

We present experimental observations on the electrically forced release of spiral waves pinned to unexcitable circular obstacles in the Belosov-Zhabotinsky reaction. When the applied electric current density reaches the necessary current density  $J_{\rm unpin}$ , the spiral tip is detached and subsequently drifts away from the obstacle.  $J_{\rm unpin}$  is found to increase with the obstacle diameter d. The growth rate  $\Delta J_{\rm unpin}/\Delta d$  is much higher for obstacles larger than the free spiral core compared to that for smaller obstacles. The experimental findings are confirmed by numerical simulations using the Oregonator model. The results imply that it is more difficult to release spiral waves pinned to larger obstacles, especially when the obstacle size exceeds that of the free spiral core.

DOI: 10.1103/PhysRevE.89.052902 PACS number(s): 05.45.-a, 05.65.+b, 82.40.Ck, 82.40.Qt

#### I. INTRODUCTION

Spiral waves evolve in different excitable media, e.g., during CO oxidation on a platinum surface [1], cell aggregation in slime mold colonies [2], electrical wave propagation in cardiac tissues [3], and concentration waves in the Belousov-Zhabotinsky (BZ) reaction [4,5]. Such spiral patterns of electrical excitation in the heart and their instabilities are involved in causing certain types of cardiac arrhythmia, such as ventricular tachycardia and fibrillations [6,7], which can potentially lead to sudden cardiac death.

Annihilation of spiral waves is possible when the waves drift until they hit the boundary of the medium. Even though this drift and annihilation can occur naturally, spiral waves in cardiac tissues are often stabilized by being pinned to local heterogeneities (e.g., veins or scars), which act as obstacles [3]. Note that obstacles may either attract or repulse spiral waves depending on the distance between the spiral core centers and the obstacles [8,9]. Furthermore, it has been predicted [10,11] that obstacles cause the period of pinned spiral waves to increase with the obstacle size. A systematic study of pinned spiral waves in a thin layer of the photosensitive ruthenium-catalyzed BZ reaction [12] has revealed that wave period, wavelength, and velocity increase with the size of a circular unexcitable obstacle created by a laser spot. For threedimensional BZ media, spiral structures known as scroll rings are often observed to contract and eventually self-annihilate [13,14]. The intrinsic contraction is suppressed, when a scroll ring is pinned to an obstacle [15,16].

It has been demonstrated that low-energy shocks, produced by virtual electrode polarization [17], can unpin and terminate ventricular tachycardia in isolated rabbit ventricles [18] and cell cultures of neonatal rat ventricular myocytes [19,20]. Other low-energy methods use a high-frequency train of electrical stimuli to eliminate spiral waves in cardiac tissue cultures by inducing unpinning and drift of the waves, until they collide with the boundary of the medium [21,22]. Such an external wave train is used to release a spiral wave pinned to a cluster of small droplets of oil in the BZ reaction [23].

In this article, we present an investigation of the electrically forced unpinning of spiral waves in BZ media. In the absence of obstacles, an applied electrical current results in an advective motion of ionic species and induces a drift of the spiral tips along a straight path. The drift velocity is found to increase with the magnitude of applied current [24–26]. Our experiments are performed in uniform thin layers of the BZ reaction [27] using chemically inert plastic cylinders with well-defined diameters as unexcitable obstacles. Thus, the relation between the strength of forcing and the obstacle size is precisely specified. We perform simulations using the Oregonator model [28,29] in close correspondence with the experimental results.

#### II. EXPERIMENTS

#### A. Methods

The Belousov-Zhabotinsky (BZ) solutions are prepared from NaBrO<sub>3</sub>, H<sub>2</sub>SO<sub>4</sub>, malonic acid (MA) and ferroin, all purchased from Merck. Stock solutions of NaBrO<sub>3</sub> (1 M) and MA (1 M) are freshly produced by dissolving powder in deionized water (conductivity of ~0.056  $\mu$ S cm<sup>-1</sup>), whereas stock solutions of H<sub>2</sub>SO<sub>4</sub> (2.5 M) and ferroin (25 mM) are commercially available. To prevent any hydrodynamic perturbation, the reaction is embedded in a 1.0% wt/wt agarose gel (Sigma). Appropriate volumes of the stock solutions are mixed and diluted in deionized water to form BZ solutions with initial concentrations: [H<sub>2</sub>SO<sub>4</sub>] = 200 mM, [MA] = 50 mM, [NaBrO<sub>3</sub>] = 50 mM, and [ferroin] = 0.625 mM. The temperature is controlled at 24 °C  $\pm$  1 °C. In the absence of electrical forcing as well as any obstacle, these BZ media

<sup>\*</sup>Corresponding author: fscicyl@ku.ac.th

support rotating spiral waves, the tip of which (measured location as in Ref. [27]) moves around a circular area (i.e., the spiral core) with a diameter of 0.75 mm. The wave period is about 4 min.

Unpinning of spiral waves by electrical forcing is studied in a uniform thin layer of the BZ reaction using a flat reactor constructed from transparent Plexiglas [27]. The volume is  $100 \times 100 \times 1.0 \text{ mm}^3$ . An electric field is applied via two electrodes in electrolytic compartments (size of each 25  $\times$  $100 \times 2.0 \text{ mm}^3$ ), which are attached to the left and the right boundaries of the main volume [14]. Application of the electric field also results in gas bubbles formed by electrolysis. The bubbles cause the resistance between the electrodes to fluctuate in time. To specify precisely the strength of forcing, electricity driven by a power supply in a constant electrical current mode is utilized, and the strength of applied electrical forcing in the experiments is recorded as electrical current density instead of electric field, which is normally used in simulations. As an obstacle, a chemically inert plastic cylinder with a diameter of 0.4-1.5 mm and a height of 1.0 mm is attached in the main volume by using silicone paste before the BZ solution is filled into the reactor. During the experiments, the reactor is placed in a transparent thermostating bath to remove Ohmic heat and to set the temperature at 24 °C  $\pm$  1 °C. The bath is put between a white light source and a color CCD camera (Super-HAD, Sony) to record the images of the medium every second with a resolution of  $0.05 \text{ mm pixel}^{-1}$ .

A spiral wave pinned to the obstacle is initiated by the following procedure: The reactor is oriented vertically, and a volume of BZ solution is filled into the reactor, forming the first layer of 2.5 cm height, where the obstacle is located. Then, we wait until the gel is formed. Wave fronts are initiated by immersion of a silver wire of 0.5 mm diameter between the left edge of the reactor and the obstacle. One open end of the wave front propagates towards the obstacle [Fig. 1(a)], while the other moves close to the left edge of the reactor. Another volume of the BZ solution is added to the reactor as the second layer when the open end reaches the obstacle [Fig. 1(b)]. The final height of the medium is about 4.5–5.0 cm. Shortly after filling in the second layer, the open end of the wave front starts to curl in [Fig. 1(c)] to form a spiral wave with its tip rotating around the obstacle [Fig. 1(d)].

#### B. Results and discussion

Figure 1 shows the development of a pinned spiral wave in our experiments. As reported earlier [27,30,31], the atmospheric oxygen suppresses the excitability of a thin sheet below the top surface of the first layer [dark orange (dark gray) band in Figs. 1(a)-1(c)], so that the wave front does not reach the atmospheric interface. After the second layer is filled, this inhibited layer disappears when the dissolved oxygen is consumed during the first passage of the excitation front [see Fig. 1(c)]. We note that filling in the BZ solution to form the second layer must be done at the proper time, i.e., when the front reaches the obstacle, as depicted in Fig. 1(b). If this is done too early or too late (i.e., when the front does not touch the obstacle), the spiral wave will not be pinned.

For obstacles larger than the free spiral core, the tips of pinned spiral waves are always attached to the obstacle [as in

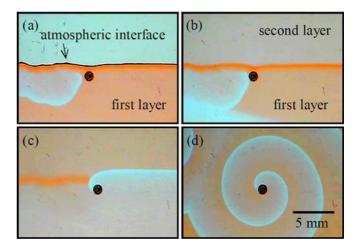


FIG. 1. (Color online) Pinning a spiral wave in the BZ reaction.

(a) A wave front is initiated by a silver wire in the first layer. (b) A portion of the BZ reaction is placed on top as the second layer, when the blue (light gray) front end reaches the obstacle (black circle; diameter of 1.05 mm). (c) The inhibited layer [dark orange (dark gray) band] disappears after the first passage of the wave front. (d) After three spiral rotations, the front adopts a typical spiral structure with its tip attached to the obstacle.

Fig. 1(d)]. In contrast, we observe alternations of attachment [Figs. 2(a) and 2(b)] and detachment [Figs. 2(c) and 2(d)] of the spiral tip in the vicinity of obstacles smaller than the free spiral core. The spiral core is an area in the refractory state, thus no wave can propagate into it. When a small obstacle occupies some part of the spiral core, the other (unoccupied) part is still in the refractory state and prohibits any wave propagation. As in Figs. 2(c) and 2(d), the spiral tip is temporarily detached from the obstacle, when it reaches such a refractory area. However, the free tip moves towards the obstacle again.

To investigate unpinning phenomena, we apply a constant current density J, which is stepwise increased from small to large values. For each value of the obstacle diameter, the

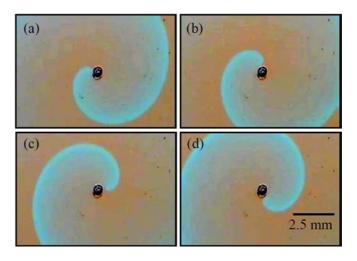


FIG. 2. (Color online) Motion of a spiral wave around a small obstacle in the BZ reaction. For each rotation, the spiral tip is alternately (a) and (b) attached to and (c) and (d) detached from the obstacle with a diameter of 0.4 mm.

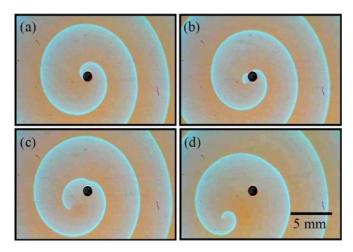


FIG. 3. (Color online) Unpinning of a spiral wave by electrical forcing in the BZ reaction. The obstacle diameter is 1.05 mm. The positive and negative electrodes are placed on the left- and the right-hand sides, respectively. (a) An electrical current density J=96 mA cm<sup>-2</sup> induces an anisotropic spiral structure with its tip still attached to the obstacle. When J reaches a critical value  $J_{\rm unpin}=98$  mA cm<sup>-2</sup>, (b) the spiral tip is detached and (c) and (d) subsequently moves away from the obstacle.

experiments are performed twice with different steps  $\Delta J = 10$  and 2 mA cm<sup>-2</sup>, respectively. In all experiments, each value of J is applied for an interval of three to five spiral rotations before J is increased. The spiral tip leaves the obstacle and moves away when J reaches a critical value  $J_{\rm unpin}$ , i.e., the minimal current density for unpinning. For guidance, the first experiment with the large step  $\Delta J = 10$  mA cm<sup>-2</sup> provides a rough estimate of electrical current density necessary for unpinning the spiral wave. The fine-tuning of J is obtained in the second experiment with  $\Delta J = 2$  mA cm<sup>-2</sup>. This way, one can obtain the finest value of  $J_{\rm unpin}$  ( $\Delta J = 2$  mA cm<sup>-2</sup>) available from our equipment within a relatively short observation time of up to 2 h, while the aging of the BZ reaction, which potentially affects the dynamics of the spiral wave in long running experiments, can be minimized.

Figure 3 demonstrates the unpinning phenomenon. With  $J < J_{\text{unpin}}$ , the spiral tip still remains attached to the obstacle. However, the forcing induces an anisotropically distorted spiral wave [see Fig. 3(a)] because the electrical current accelerates or decelerates the front propagating towards or away from the positive electrode [26], while the spiral tip remains pinned. For  $J \ge J_{\text{unpin}}$ , the spiral tip is detached from the obstacle [see Fig. 3(b)]. When the electrical current is continuously applied, the unpinned spiral tip moves towards the positive electrode with an angle. The anisotropic structure also changes with time [see Figs. 3(b)–3(d)]. As the spiral tip moves far away from the obstacle [Fig. 3(d)], we observed the deformed wave structure similar to a drifting spiral wave under electrical forcing in the absence of obstacles [24].

The necessary current density  $J_{\rm unpin}$  for unpinning the spiral wave increases with the obstacle diameter d, as shown in Fig. 4. For obstacles smaller than the free spiral core (d < 0.75 mm),  $J_{\rm unpin}$  increases with d, but the increase is slower than that for larger obstacles (d > 0.75 mm). To investigate the growth rate  $\Delta J_{\rm unpin}/\Delta d$ , we apply linear fits for the two ranges of the

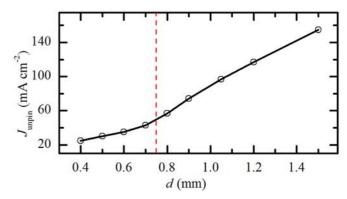


FIG. 4. (Color online) Electrical current density  $J_{\rm unpin}$  necessary for releasing a spiral wave pinned to an unexcitable obstacle with diameter d. The vertical dashed line at 0.75 mm indicates the core diameter of a free spiral wave.

obstacle diameter and find that  $\Delta J_{\rm unpin}/\Delta d=0.590\pm0.052$  and  $1.389\pm0.048~{\rm A~cm^{-3}}$  for  $d<0.75~{\rm mm}$  and  $d>0.75~{\rm mm}$ , respectively. Clearly,  $J_{\rm unpin}$  grows at a much higher rate for the large obstacles in comparison with that for the small ones. The results show that it is more difficult to release spiral waves pinned to larger obstacles, especially when the obstacle size exceeds that of the free spiral core.

#### III. SIMULATIONS

#### A. Methods

In our numerical simulations, we use the two-variable Oregonator model to describe the dynamics of the activator u and the inhibitor v (corresponding to the concentrations of HBrO<sub>2</sub> and the catalyst, respectively) in the BZ reaction. The advection terms for both u and v account for the electric field E applied in the x direction:

$$\frac{\partial u}{\partial t} = \frac{1}{\varepsilon} \left( u - u^2 - f v \frac{u - q}{u + q} \right) + D_u \nabla^2 u - M_u E \frac{\partial u}{\partial x},$$

$$\frac{\partial v}{\partial t} = u - v + D_v \nabla^2 v - M_v E \frac{\partial v}{\partial x}.$$
(1)

As in Refs. [14,29], the parameters are chosen as  $\varepsilon = 0.01$ , q = 0.002, f = 1.4, the diffusion coefficients  $D_u = 1.0$  and  $D_v = 0.6$ , and the ionic mobilities  $M_u = -1.0$  and  $M_v = 2.0$ . In the absence of an electric field, the tip of a free spiral wave rotates around a circular core [diameter = 0.9 system unit (s.u.)]. The spiral tip is defined as the intersection of the contour u = 0.15 and v = 0.0935 to ensure  $\partial u/\partial t = 0$  on the position of the tip [14].

The simulations are performed using an explicit Euler method with a nine-point approximation of the two-dimensional Laplacian operator and a centered-space approximation of the gradient term. The uniform grid space  $\Delta x = \Delta y = 0.025$  s.u. and the time step  $\Delta t = 1.9 \times 10^{-4}$  time unit (t.u.) are chosen as required for numerical stability  $[\Delta t \le (3/8)(\Delta x)^2 \ [32]]$ . The dimensionless size of the system is  $20 \times 20$  s.u. (corresponding to  $800 \times 800$  grid points). A completely unexcitable circular area is put as the obstacle. Therefore, the boundaries of both the medium and the obstacle have no-flux conditions.

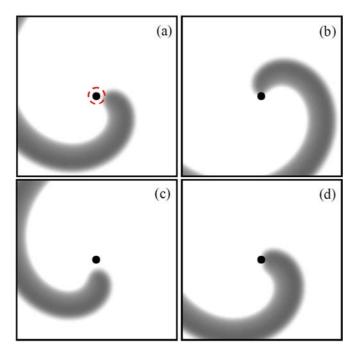


FIG. 5. (Color online) Motion of a spiral wave around a small obstacle in the Oregonator model. (a) At the beginning, an obstacle 0.5 s.u. in diameter is put in the middle of the spiral core (the dashed circle). (b) The tip moves towards and is attached to the obstacle. (c) Subsequently, it is detached from the obstacle, but (d) it is attached to the obstacle again.

To create a spiral wave, a planar wave is triggered by setting a five-grid-point strip at an edge of the medium to an excited state (e.g., u = 1.0 and v = 0 for  $0.0 \le x \le 0.5$ ). The wave front is allowed to propagate into the middle of the medium before half of the medium is reset to an excitable state (e.g., u = 0 and v = 0 for  $0.0 \le v \le 10.0$ ), leading to a free-end

wave front, which subsequently curls to form a rotating spiral wave. The circular obstacle (diameter d of 0.2–1.9 s.u.) is put in the middle of the spiral core after the spiral wave is allowed to propagate freely for several rotations.

#### B. Results and discussion

The obstacles affect the movement of the spiral tip in the same ways as found in our experiments. In the case of large obstacles, the spiral tip is simply attached to the obstacle at all times. However, alternations of attachment and detachment of the spiral tip to the obstacle smaller than the free spiral core are observed. Figure 5 illustrates the dynamics of the spiral tip in the vicinity of such a small obstacle with d=0.5 s.u. Shortly after the obstacle is put into the spiral core [see Fig. 5(a)], the spiral tip leaves its circular path (the dashed circle) and moves closer to the obstacle until getting attached to it [Fig. 5(b)]. Subsequently, the spiral tip is detached from the obstacle and moves away for a short distance [Fig. 5(c)] before moving back and being attached to the obstacle again [Fig. 5(d)].

As in our experimental results, the pinned spiral wave in the simulations is forced to drift away from the obstacle only when the applied electric field E reaches the critical value  $E_{\rm unpin}$  (the electric field necessary for unpinning). Figure 6 demonstrates the dynamics of a pinned spiral wave under the applied field. When E=0.625, which is very close to but weaker than  $E_{\rm unpin}$ , the spiral tip is alternately detached from [Figs. 6(a), 6(b), and 6(d)] and attached to [Figs. 6(c) and 6(e)] the obstacle.

The unpinning is successful at a slightly stronger field E = 0.630. At the beginning, the motion of the spiral tip seems similar to that at the weaker field [compare Figs. 6(a) and 6(b) with 6(a') and 6(b')]. On collision with the obstacle in Figs. 6(b) and 6(b'), a part of the front end (indicated by the arrows) is separated from the spiral wave. For E = 0.625, this small segment of the broken front end contracts until it

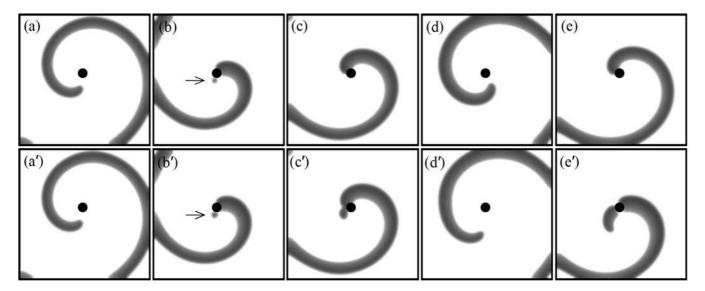


FIG. 6. Effect of an electrical field on a pinned spiral wave in the Oregonator model. The obstacle diameter is 1.5 s.u. The direction of the electric field E is pointing to the right of the images. (a)–(e) Forced temporary detachments: The spiral tip is alternately attached to and detached from the obstacle under E = 0.625. (a')–(e') Unpinning: The spiral tip is detached and moves away from the obstacle under E = 0.630. The arrows indicate the segments of broken front end.

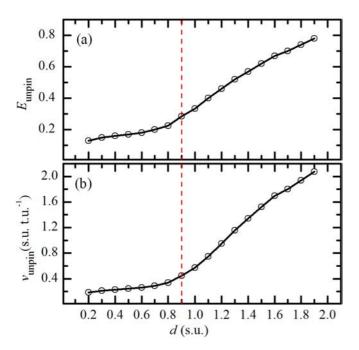


FIG. 7. (Color online) Necessary forcing to release a spiral wave pinned to an unexcitable obstacle with diameter d in the Oregonator model: (a) the electrical field  $E_{\rm unpin}$  and (b) the corresponding drift velocity  $v_{\rm unpin}$ . The vertical dashed line at 0.9 s.u. indicates the core diameter of a free spiral wave.

disappears, so that the spiral wave is attached to the obstacle again [Fig. 6(c)]. In contrast, this segment grows at E=0.630 and subsequently merges to the spiral structure, so that the spiral tip does not touch the obstacle [Fig. 6(c')]. The spiral tip drifts farther away from the obstacle over the course of time [see Figs. 6(a')-6(e')]; that is, the spiral wave is successfully unpinned from the obstacle.

The simulations not only reproduce the forced unpinning in our experiments but also reveal the forced temporary detachments around large obstacles [e.g., Figs. 6(a)–6(e)], which are not observed in the BZ reaction. We conjecture that the finest step of the electrical current density ( $\Delta J = 2$  mA cm<sup>-2</sup>) might be insufficiently small to allow these phenomena to occur in our experiments.

Figure 7(a) depicts the necessary applied field  $E_{\rm unpin}$  to unpin the spiral wave for different obstacle diameters d. Linear fits provide an approximation of the growth rate  $\Delta E_{\rm unpin}/\Delta d=0.145\pm0.011$  and  $0.501\pm0.016$  s.u.  $^{-1}$  for d<0.9 s.u. and d>0.9 s.u. This increment of  $E_{\rm unpin}$  with a much higher rate for obstacles larger than the free spiral core agrees well with the experiments (Fig. 4). To generalize the forcing, we performed additional simulations by applying the electric field  $E_{\rm unpin}$  [the same values as in Fig. 7(a)] to a free spiral wave (without obstacle) and measured the corresponding drift velocity ( $v_{\rm unpin}$ ) of the spiral tip. As shown in Fig. 7(b), the

dependence of  $v_{\rm unpin}$  on the obstacle size is similar to that of  $E_{\rm unpin}$ : the growth rate  $\Delta v_{\rm unpin}/\Delta d=0.227\pm0.022$  and  $1.69\pm0.045~{\rm s.u.}^{-1}$  for  $d<0.9~{\rm s.u.}$  and  $d>0.9~{\rm s.u.}$ 

The systematic studies in both experiments (Fig. 4) and simulations (Fig. 7) show that unpinning of spiral waves occurs under relative small forcing, when the obstacles are smaller than the free spiral core. This may be because the spiral tip is not tightly attached to those small obstacles: Its temporary detachments occur when the tip reaches the refractory area (Figs. 2 and 5) even in the absence of external forcing. In contrast, the spiral tip always touches larger obstacles.

Our investigation shows that stronger electrical forcing is needed for unpinning a spiral wave from a larger unexcitable obstacle in chemical media. This requirement of sufficient electrical forcing is consistent with earlier studies on unpinning by an external wave train [11,23,33], where the unpinning is successful only when the frequency of the wave train is higher than the critical value, which increases with the obstacle size. Since the highest frequency of waves is limited by the refractory time of the excitable medium, such unpinning is impossible when the obstacle is very large [11,23]. For some conditions, the pinned spiral wave can be released by the wave train only when the obstacle is smaller than the free spiral core [33]. It is demonstrated [33–35] that the situations can be improved by reducing the excitability of the medium, which leads to an enlargement of the spiral core size.

#### IV. CONCLUSIONS

We have presented an investigation of the release of a pinned spiral wave in the BZ reaction by electrical forcing. Under a small electrical current density, the spiral wave still remains pinned to an unexcitable cylindrical obstacle. When the electrical current density reaches a critical threshold, the spiral wave is released. The critical current density increases linearly stepwise with the diameter of the obstacle: it grows at a much higher rate for obstacles larger than the free spiral core in comparison to that of smaller obstacles. The experimental results are confirmed by simulations using the Oregonator model. From both parts of this study, we conclude that a release of a pinned spiral wave by an electric forcing is feasible for obstacle sizes both smaller and larger than the free spiral core. However, the study of such electrically forced unpinning becomes a tough endeavor when the wave is pinned to an obstacle larger than the free spiral core.

#### ACKNOWLEDGMENTS

We thank the Faculty of Science, the Research and Development Institute (KURDI), the Center for Advanced Studies of Industrial Technology, and the Graduate School, Kasetsart University; the German Academic Exchange Service (DAAD); and the Thailand Research Fund (Grant No. TRG5680044) for financial support.

S. Nettesheim, A. von Oertzen, H. H. Rotermund, and G. Ertl, J. Chem. Phys. 98, 9977 (1993).

<sup>[2]</sup> F. Siegert and C. J. Weijer, J. Cell Sci. 93, 325 (1989).

<sup>[3]</sup> J. M. Davidenko, A. M. Pertsov, R. Salomonz, W. Baxter, and J. Jalife, Nature (London) 355, 349 (1992).

<sup>[4]</sup> A. T. Winfree, Science 175, 634 (1972).

<sup>[5]</sup> A. T. Winfree, Science 181, 937 (1973).

<sup>[6]</sup> A. T. Winfree, Science 266, 1003 (1994).

<sup>[7]</sup> E. M. Cherry and F. H. Fenton, New J. Phys. 10, 125016 (2008).

- [8] A. P. Muñuzuri, V. Pérez-Muñuzuri, and V. Pérez-Villar, Phys. Rev. E 58, R2689 (1998).
- [9] C. W. Zemlin and A. M. Pertsov, Phys. Rev. Lett. 109, 038303 (2012).
- [10] J. P. Keener and J. J. Tyson, Physica D (Amsterdam, Neth.) 21, 307 (1986).
- [11] Y.-Q. Fu, H. Zhang, Z. Cao, B. Zheng, and G. Hu, Phys. Rev. E 72, 046206 (2005).
- [12] O. Steinbock and S. C. Müller, Physica A (Amsterdam, Neth.) 188, 61 (1992).
- [13] K. I. Agladze, R. A. Kocharyan, and V. I. Krinsky, Physica D (Amsterdam, Neth.) 49, 1 (1991).
- [14] C. Luengviriya, S. C. Müller, and M. J. B. Hauser, Phys. Rev. E 77, 015201 (2008).
- [15] Z. Jiménez, B. Marts, and O. Steinbock, Phys. Rev. Lett. 102, 244101 (2009).
- [16] Z. Jiménez and O. Steinbock, Europhys. Lett. 91, 50002 (2010).
- [17] I. R. Efimov, Y. N. Cheng, M. Biermann, D. R. Van Wagoner, T. Mazgalev, and P. J. Tchou, J. Cardiovasc. Electrophysiol. 8, 1031 (1997).
- [18] C. M. Ripplinger, V. I. Krinsky, V. P. Nikolski, and I. R. Efimov, Am. J. Physiol. Heart Circ. Physiol. 291, 184 (2006).
- [19] J. Cysyk and L. Tung, Biophys. J. 94, 1533 (2008).
- [20] M. Hörning, A. Isomura, K. Agladze, and K. Yoshikawa, Phys. Rev. E 79, 026218 (2009).
- [21] K. Agladze, M. W. Kay, V. Krinsky, and N. Sarvazyan, Am. J. Physiol. Heart Circ. Physiol. 293, 503 (2007).

- [22] A. Isomura, M. Hörning, K. Agladze, and K. Yoshikawa, Phys. Rev. E 78, 066216 (2008).
- [23] M. Tanaka, A. Isomura, M. Hörning, H. Kitahata, K. Agladze, and K. Yoshikawa, Chaos 19, 043114 (2009).
- [24] O. Steinbock, J. Schütze, and S. C. Müller, Phys. Rev. Lett. **68**, 248 (1992).
- [25] K. I. Agladze and P. De Kepper, J. Phys. Chem. **96**, 5239 (1992).
- [26] A. P. Muñuzuri, V. A. Davydov, V. Pérez-Muñuzuri, M. Gómez-Gesteira, and V. Pérez-Villar, Chaos Solitons Fractals 7, 585 (1996).
- [27] C. Luengviriya, U. Storb, M. J. B. Hauser, and S. C. Müller, Phys. Chem. Chem. Phys. 8, 1425 (2006).
- [28] R. J. Field and R. M. Noyes, J. Chem. Phys. **60**, 1877 (1974).
- [29] W. Jahnke and A. T. Winfree, Int. J. Bifurcation Chaos Appl. Sci. Eng. 1, 445 (1991).
- [30] A. F. Taylor, B. R. Johnson, and S. K. Scott, J. Chem. Soc. Faraday Trans. 94, 1029 (1998).
- [31] A. F. Taylor, B. R. Johnson, and S. K. Scott, Phys. Chem. Chem. Phys. 1, 807 (1999).
- [32] M. Dowle, R. M. Mantel, and D. Barkley, Int. J. Bifurcation Chaos Appl. Sci. Eng. **7**, 2529 (1997).
- [33] A. Pumir, S. Sinha, S. Sridhar, M. Argentina, M. Hörning, S. Filippi, C. Cherubini, S. Luther, and V. Krinsky, Phys. Rev. E 81, 010901(R) (2010).
- [34] Z. Y. Lim, B. Maskara, F. Aguel, R. Emokpae, and L. Tung, Circulation. 114, 2113 (2006).
- [35] C. Cabo, A. M. Pertsov, J. M. Davidenko, W. T. Baxter, R. A. Gray, and J. Jalife, Biophys. J. 70, 1105 (1996).

#### PHYSICAL REVIEW E 91, 052912 (2015)

#### Propagation of spiral waves pinned to circular and rectangular obstacles

Malee Sutthiopad, <sup>1</sup> Jiraporn Luengviriya, <sup>2,3</sup> Porramain Porjai, <sup>1</sup> Metinee Phantu, <sup>1</sup> Jarin Kanchanawarin, <sup>3</sup> Stefan C. Müller, <sup>4</sup> and Chaiya Luengviriya<sup>1,\*</sup>

<sup>1</sup>Department of Physics, Kasetsart University, 50 Phaholyothin Road, Jatujak, Bangkok 10900, Thailand <sup>2</sup>Department of Industrial Physics and Medical Instrumentation, King Mongkut's University of Technology North Bangkok, 1518 Pibulsongkram Road, Bangkok 10800, Thailand

<sup>3</sup>Lasers and Optics Research Group, King Mongkut's University of Technology North Bangkok, 1518 Pibulsongkram Road, Bangkok 10800, Thailand

<sup>4</sup>Institute of Experimental Physics, Otto-von-Guericke University Magdeburg, Universitätsplatz 2, D-39106 Magdeburg, Germany (Received 5 March 2015; published 15 May 2015)

We present an investigation of spiral waves pinned to circular and rectangular obstacles with different circumferences in both thin layers of the Belousov-Zhabotinsky reaction and numerical simulations with the Oregonator model. For circular objects, the area always increases with the circumference. In contrast, we varied the circumference of rectangles with equal areas by adjusting their width w and height h. For both obstacle forms, the propagating parameters (i.e., wavelength, wave period, and velocity of pinned spiral waves) increase with the circumference, regardless of the obstacle area. Despite these common features of the parameters, the forms of pinned spiral waves depend on the obstacle shapes. The structures of spiral waves pinned to circles as well as rectangles with the ratio  $w/h \sim 1$  are similar to Archimedean spirals. When w/h increases, deformations of the spiral shapes are observed. For extremely thin rectangles with  $w/h \gg 1$ , these shapes can be constructed by employing semicircles with different radii which relate to the obstacle width and the core diameter of free spirals.

DOI: 10.1103/PhysRevE.91.052912 PACS number(s): 05.45.—a, 05.65.+b, 82.40.Ck, 82.40.Qt

#### I. INTRODUCTION

Propagating spiral waves have been discovered in various reaction-diffusion systems such as CO oxidation on platinum surfaces [1], cell aggregation in slime mold colonies [2], electrical wave propagation in cardiac tissues [3], and concentration waves in the Belousov-Zhabotinsky (BZ) reaction [4,5]. In the heart, electrical spiral waves are connected with cardiac tachycardia and life-threatening fibrillations [6,7]. Such spiral waves may cease when their tip hits the boundary of the medium. However, they will survive much longer if they are pinned to anatomical inhomogeneities or obstacles, e.g., veins or scars [3].

Unexcitable disks have been widely taken as model obstacles to study the effects of obstacle size on the properties of spiral waves pinned to them. Tyson and Keener's theoretical work [8] predicted that a spiral wave rotating around a circular hole has period and velocity that increase when the hole is enlarged. Tanaka et al. [9] proposed a formula which showed that the spiral wave velocity at the periphery of the circular obstacle increases with the obstacle radius. Simulations by Fu et al. [10] revealed that both unexcitable and partially excitable circles cause the period of spiral waves to increase with their radii. Similarly, Cherubini et al. [11] showed that the wavelength and the period also increase linearly with the obstacle radius in cardiac model systems, regardless of whether the elasticity of the medium was included in the simulations. For spiral waves in cardiomyocytes, their velocity and wavelength were found to increase linearly with the circumference of the circular obstacle [12].

Experiments using thin layers of the photosensitive ruthenium-catalyzed BZ reaction [13] have demonstrated that

wave period, wavelength, and velocity of a spiral wave increased from 26 s, 1.3 mm, and 49.6  $\mu$ m s<sup>-1</sup> to 49 s, 3.4 mm, and 74.3  $\mu$ m s<sup>-1</sup>, respectively, after an artificial circular core was created by a laser spot of 1.2 mm in diameter. A scroll ring (i.e., a spiral structure in three dimensions) has been often observed to contract and eventually self-annihilate [14,15]. However, the contraction was suppressed when the scroll ring was pinned to spherical plastic beads [16,17].

In this article, we present an investigation of the dynamics of pinned spiral waves in BZ media. We chose two different simple forms of obstacles: circles and rectangles. Circles are symmetric objects which were used in many studies of pinned spiral waves in experiments and simulations, whereas rectangles have the advantage that their width and height are adjustable to obtain different circumferences while the area can be fixed to a constant value. We confirmed our experimental results by numerical simulations using the Oregonator model [18,19].

#### II. EXPERIMENTS

#### A. Experimental methods

We prepared the Belousov-Zhabotinsky (BZ) solutions from NaBrO<sub>3</sub>, H<sub>2</sub>SO<sub>4</sub>, malonic acid (MA), and ferroin, all purchased from Merck. Stock solutions of NaBrO<sub>3</sub> (1 M) and MA (1 M) were freshly produced by dissolving powder in deionized water (conductivity  $\sim 0.056~\mu S~cm^{-1}$ ), whereas stock solutions of H<sub>2</sub>SO<sub>4</sub> (2.5 M) and ferroin (25 mM) were commercially available. To prevent any hydrodynamic perturbation, the reaction was embedded in a 1.0% w/w agarose gel (Sigma). Appropriate volumes of the stock solutions were mixed and diluted in deionized water to form BZ solutions with initial concentrations: [H<sub>2</sub>SO<sub>4</sub>] = 160 mM,

<sup>\*</sup>Corresponding author: fscicyl@ku.ac.th

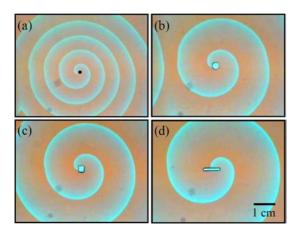


FIG. 1. (Color online) Spiral waves in the BZ reaction: (a) A free spiral wave (no obstacle) with a spiral core of 1.0 mm diameter (black circle), and spiral waves pinned to (b) a circle with diameter 2.8 mm and to rectangles with dimensions (c) 2.3 mm  $\times$  2.6 mm and (d) 6.5 mm  $\times$  0.9 mm.

[MA] = 50 mM, [NaBrO<sub>3</sub>] = 50 mM, and [ferroin] = 0.625 mM. At a temperature of 15 °C, the BZ solutions supported spiral waves with wavelength, period, and velocity of 7.5 mm,  $11.4 \, \text{min}$ , and  $0.66 \, \text{mm min}^{-1}$ , respectively.

The influence of unexcitable obstacles on the propagation of spiral waves (shown, e.g., in Fig. 1) was investigated in a uniform thin layer of the BZ reaction using a flat reactor (volume  $100 \times 100 \times 1.0 \text{ mm}^3$ ) constructed from transparent Plexiglas [20]. Eight circles with different diameters of 1.5, 1.9, 2.5, 2.8, 3.1, 3.5, 3.9, and 4.5 mm and four rectangles with width and height of  $2.3 \times 2.6$ ,  $4.6 \times 1.3$ ,  $4.9 \times 1.2$ , and  $6.5 \times 0.9 \text{ mm}^2$  were created also from Plexiglas plates (thickness 1.0 mm, the same as for the BZ layers) using a computerized laser cutting machine [see Figs. 1(b)–1(d) for examples of the obstacles]. The area A and the circumference l of circular and rectangular obstacles are summarized in Fig. 2(a). In each experiment, one obstacle was attached in the reactor before filling in the BZ solution.

A spiral wave pinned to an obstacle was initiated by a two-layer method as demonstrated earlier (cf. Fig. 1 in Ref. [21]). During the observations, the reactor was placed in a transparent thermostatting bath to control the temperature at  $15 \pm 0.1$  °C. The bath was set between a white light source and a color charge-coupled-device camera (Super-HAD, Sony) to record the images of the spiral wave every second with a resolution of 0.10 mm pixel<sup>-1</sup>. The wavelength, the period, and the velocity of spiral fronts were measured at locations at least one wavelength away from the tip of free spirals or from the obstacle edges to which the spirals were pinned to avoid the curvature effect as described in an earlier work [22].

It is worth noting that a difficulty of this experimental investigation comes from the long period of pinned spiral waves and emergences of undesired circular waves and free spirals that are often generated by some sources, like dust particles, in the BZ reaction. Due to their shorter period, these waves, especially the free spirals, interact and subsequently overcome the pinned spiral waves after some time, as mentioned earlier by Steinbock and Müller in Ref. [13]. If such undesired waves occur, by chance,

near the obstacles and the structure of pinned spiral wave is perturbed, the measurement criterion described above cannot be fulfilled. In this case, the experiments were repeated with new preparations of the BZ reaction. Therefore, carefully cleaning of the reactor as well as the obstacles before the experiments should be done to minimize the undesired waves.

#### **B.** Experimental results

Figure 1 illustrates examples of spiral waves with different wavelengths observed in our experiments. In the absence of obstacles, the BZ solutions supported spiral waves with wavelength  $\lambda=7.5$  mm and the spiral tip (measured location as in Ref. [20]) traced a circular area of 1.0 mm in diameter, as in Fig. 1(a). Spiral waves pinned to obstacles having a similar area of about 6 mm² but differing in shape and circumference l are shown in Figs. 1(b)–1(d). The wavelength  $\lambda$  was enlarged to 14.3 mm for the case of a circle with diameter 2.8 mm [l=8.8 mm, Fig. 1(b)]. A similar wavelength ( $\lambda=14.4$  mm) was observed for the rectangle with dimensions 2.3 mm  $\times$  2.6 mm [l=9.8 mm, Fig. 1(c)]. The longer rectangle with dimensions 6.5 mm  $\times$  0.9 mm [l=14.8 mm, Fig. 1(d)] resulted in a much larger wavelength of 20.3 mm.

Figure 2 summarizes the properties of pinned spiral waves as well as obstacles investigated in our experiments. Since free spiral waves in the BZ solutions rotated around a circular core with diameter of 1.0 mm, we considered the core as a circular obstacle and included the properties of the free spirals

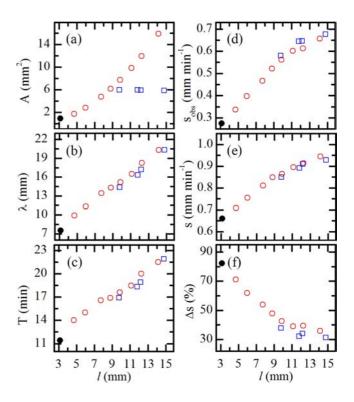


FIG. 2. (Color online) Properties of spiral waves as a function of the obstacle circumference l in the BZ reaction: (a) obstacle area A, (b) wavelength  $\lambda$ , (c) wave period T, [(d) and (e)] velocities  $s_{\rm obs}$  and s of waves adjacent to and far from the obstacles, respectively, and (f) percentage difference  $\Delta s$  between  $s_{\rm obs}$  and s. Filled circles: no physical obstacles (spiral core diameter 1.0 mm); open circles: circular obstacles; open rectangles: rectangular obstacles.

in Fig. 2 (see filled circles) for the purpose of comparison. Figure 2(a) shows the relation between area and circumference of the obstacles. As the diameter increases from 1.0 to 4.5 mm, the circumference l and the area A of the circles increase simultaneously from 3.1 to 14.1 mm and 0.8 to 15.9 mm², respectively. In contrast, the four rectangles  $(2.3 \times 2.6, 4.6 \times 1.3, 4.9 \times 1.2, \text{ and } 6.5 \times 0.9 \text{ mm}^2)$  with a circumference l ranging between 9.8 and 14.8 mm have almost the same area size of about 6 mm².

The spiral waves propagated around the obstacles with wavelength  $\lambda$  [Fig. 2(b)] and wave period T [Fig. 2(c)] increasing with the obstacle circumference l in both the cases of circles and rectangles. Moreover, data points from all obstacles lay approximately on the same line of each graph. The growth rate of the wavelength and the period with respect to the circumference are estimated by linear fits as  $\lambda/l = 1.064$  $\pm 0.043$  and  $T/l = 0.806 \pm 0.047$  min mm<sup>-1</sup>. To investigate the influence of the obstacles on the velocity of the spiral waves, we calculated the average velocity of the wave ends attached to the obstacles  $s_{obs}$  as the ratio between the circumference and the period  $s_{\text{obs}} = l/T$  as well as that of the spiral fronts far away from the obstacles s as the ratio between the wavelength and the period  $s = \lambda/T$ . As shown in Figs. 2(d) and 2(e), both  $s_{obs}$ and s increase with l. Even though  $s_{obs}$  is always smaller than s for a given obstacle, its growth rate of  $s_{\rm obs}$  ( $s_{\rm obs}/l = 0.037 \pm$  $0.002 \, \mathrm{min}^{-1}$ ) is larger than that of  $s \, (s/l = 0.024 \pm 0.002)$  $\min^{-1}$ ). Therefore, their percentage difference [ $\Delta s(\%)$  =  $|s_{\rm obs} - s|/(s_{\rm obs} + s)/2 \times 100$ ] becomes smaller, while the circumference increases, as indicated in Fig. 2(f).

The structure of pinned spiral waves is also affected by the obstacles, as shown in Fig 3. During their evolution around circles, the spiral shape remains unchanged all the time and is well fitted by an Archimedean spiral [Fig. 3(a)]. For a rectangle with the width w similar to the height h (i.e., w/h = 0.9), the pinned spiral wave still looks similar to an Archimedean spiral [Fig. 3(b)]. When the ratio w/h of the rectangle is increased (i.e., to a more asymmetric shape), the spiral deviates farther from an Archimedean one [e.g., in Fig. 3(c) with w/h = 7.2]. In fact, the observed structures differ from any other mathematical spiral known to us (i.e., Euler's, Fermat's, hyperbolic, logarithmic spirals, etc.). These unusual spiral shapes also change periodically, while the waves rotate around the obstacles. As shown in Fig. 3(c),

the wave front near the obstacle has a high curvature when the wave end turns around the short boundaries on the left and the right. As the wave end propagates further along the long edges (the upper and the lower walls), the curvature of the nearby front continually decreases. A description of a spiral wave pinned to a rectangle similar to Fig. 3(c), but with extremely high w/h, is given in the section of simulation results (see Figs. 7 and 8).

#### III. SIMULATIONS

#### A. Simulation methods

Numerical simulations have been performed using the two-variable Oregonator model, as in Eq. (1), to describe the dynamics of the activator u and the controller v which account for the concentrations of HBrO<sub>2</sub> and the catalyst in the BZ reaction, respectively,

$$\frac{\partial u}{\partial t} = \frac{1}{\varepsilon} \left( u - u^2 - f v \frac{u - q}{u + q} \right) + D_u \nabla^2 u,$$

$$\frac{\partial v}{\partial t} = u - v + D_v \nabla^2 v.$$
(1)

As in a study by Jahnke and Winfree [19], the parameters were chosen as  $\varepsilon = 0.01$ , q = 0.002, f = 1.4, and the diffusion coefficients as  $D_u = 1.0$  and  $D_v = 0.6$ . For this parameter set, the system supported spiral waves with a circular spiral core of 0.9 space units (s.u.) in diameter, wavelength = 10.5 s.u., period = 1.55 time units (t.u.), and velocity = 6.76 s.u. t.u.<sup>-1</sup>.

The variables u and v in Eq. (1) were calculated using an explicit Euler method with a nine-point approximation of the two-dimensional Laplacian operator on a discrete system of a dimensionless size =  $160 \times 160$  s.u. with a uniform grid space of  $\Delta x = \Delta y = 0.1$  s.u. and a time step  $\Delta t = 3.0 \times 10^{-3}$  t.u., as required for numerical stability [ $\Delta t < (3/8)(\Delta x)$ ]<sup>2</sup> [23]). A single unexcitable circle or rectangle was defined as the obstacle in each simulation. The boundaries of both the medium and the obstacle had no-flux conditions. The implementation of a circular obstacle with no-flux boundary was described in a recent publication [24]. We tested totally 10 circles with different diameters of 1.5, 2.0, 3.0, 4.0, 5.0, 6.0, 7.0, 8.0, 9.0, and 10.0 s.u. and six rectangles with widths

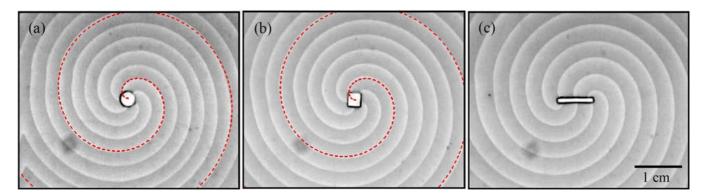


FIG. 3. (Color online) Image overlays of counterclockwise rotating spiral waves pinned to (a) a circle with diameter 2.8 mm and to rectangles with dimensions (b)  $2.3 \text{ mm} \times 2.6 \text{ mm}$  and (c)  $6.5 \text{ mm} \times 0.9 \text{ mm}$  in the BZ reaction. Dashed curves in (a) and (b) are Archimedean spirals with origins located at the obstacle centers.

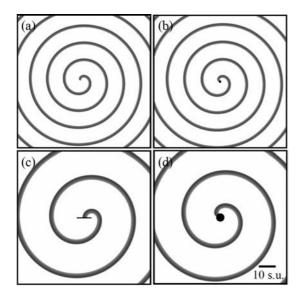


FIG. 4. Spiral waves in the Oregonator model: (a) a free spiral wave (no obstacle, spiral core diameter 0.9 s.u.) and spiral waves pinned to (b) a circle with diameter of 1.5 s.u., (c) a rectangle with dimensions  $8.5 \, \text{s.u.} \times 0.2 \, \text{s.u.}$  and (d) a circle with diameter of  $5.0 \, \text{s.u.}$ 

and heights of 1.3  $\times$  1.3, 1.7  $\times$  1.0, 3.4  $\times$  0.5, 5.4  $\times$  0.3, 8.5  $\times$  0.2, and 17.0  $\times$  0.1 s.u.<sup>2</sup>.

To create a spiral wave pinned to an obstacle, a planar wave was triggered by setting a five-grid-point strip at the left edge of the medium to an excited state (e.g., u=1.0 and v=0 for  $0.0 \leqslant x \leqslant 0.5$ ). When the wave front reached the obstacle (around the middle of the medium), half of the medium was reset to an excitable state (e.g., u=0 and v=0 for  $80.0 \leqslant y \leqslant 160.0$ ), leading to a planar wave with two ends attached to the edges of the obstacle and the system. Subsequently, the wave front curled to form a pinned spiral wave rotating around the obstacle (cf. Fig. 1 in Ref. [21]).

#### **B.** Simulation results

Examples of spiral waves with wavelengths depending on the obstacle circumference in the Oregonator model are shown in Fig. 4. A free spiral wave, as in Fig. 4(a), has a wavelength  $\lambda = 10.5$  s.u. and its tip rotates around a circular core (diameter 0.9 s.u.). Spiral waves pinned to three different obstacles are shown in Figs. 4(b)-4(d). A small circle with a diameter of 1.5 s.u. (area A = 1.77 s.u.<sup>2</sup>, circumference l = 4.7 s.u.), in Fig. 4(b), caused a small expansion of the wavelength to 10.7 s.u., while a rectangle with dimensions 8.5 s.u.  $\times$  0.2 s.u. with a smaller area  $A = 1.70 \text{ s.u.}^2$ , but a much longer l = 17.4 s.u., in Fig. 4(c), resulted in a spiral wave with a wavelength  $\lambda$  = 20.7 s.u. In Fig. 4(d), a pinned spiral wave with a wavelength  $\lambda = 20.2$  s.u., similar to that in Fig. 4(c), was obtained from a circular obstacle with a diameter of 5.0 s.u. having a similar circumference (l = 15.7 s.u.) but much larger area (A = 19.64 s.u.<sup>2</sup>) in comparison to the rectangle in Fig. 4(c).

The properties of pinned spiral waves and obstacles in our simulations are presented in Fig. 5. As in the experimental part, the free spiral waves were taken as if they were pinned to a circular obstacle with diameter of 0.9 s.u. and their properties

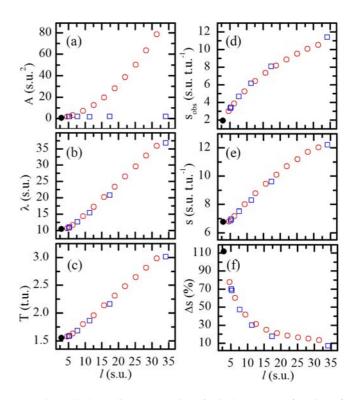


FIG. 5. (Color online) Properties of spiral waves as a function of the obstacle circumference l in the Oregonator model: (a) obstacle area A, (b) wavelength  $\lambda$ , (c) wave period T, [(d) and (e)] velocities  $s_{\rm obs}$  and s of waves adjacent to and far from the obstacles, respectively, and (f) percentage difference  $\Delta s$  of  $s_{\rm obs}$  and s. Filled circles: no physical obstacles (spiral core diameter 0.9 s.u.); open circles: circular obstacles; open rectangles: rectangular obstacles.

were included in this figure (see the filled circles). The obstacle areas A with different circumferences l are shown in Fig. 5(a). For the circular obstacles, the circumference l and the area A increase simultaneously from 3.0 to 31.4 s.u. and 0.71 to 78.55 s.u.<sup>2</sup>, respectively, when the diameter increases from 0.9 to 10.0 s.u. In contrast, the six rectangles with circumferences l between 5.2 and 34.2 s.u. have similar area sizes of 1.62-1.70 s.u.<sup>2</sup>. As shown in Figs. 5(b)-5(f), both circular and rectangular obstacles affected the properties of simulated spiral waves in the same manner as found in the experiments. The wavelength  $\lambda$  and the period T increase monotonously with a growth rate of  $\lambda/l = 0.921 \pm 0.020$  and  $T/l = 0.052 \pm$ 0.001 t.u. s.u.<sup>-1</sup>. For a given obstacle, the waves adjacent to the obstacle always propagate slower than the waves far from the obstacle ( $s_{\rm obs} < s$ ) but the rate  $s_{\rm obs}/l = 0.288 \pm 0.015$ t.u.<sup>-1</sup> is larger than  $s/l = 0.195 \pm 0.006$  t.u.<sup>-1</sup>. Thus, the percentage difference  $\Delta s$  of the velocities decreases, while the circumference increases.

Figure 6 illustrates examples of spiral structures for different obstacles. For circles and squares (i.e., the ratio of width and height w/h = 1.0), the shape of the spiral waves is approximated by Archimedean spirals, as in Figs. 6(a) and 6(b), respectively. For other rectangles with w/h > 1, the spiral waves adapt to unusual shapes, which change periodically as observed in our experiments. Figure 6(c) depicts a spiral wave rotating around a rectangle with extremely high w/h of 170. Shortly after the spiral performs a narrow U turn at the left and

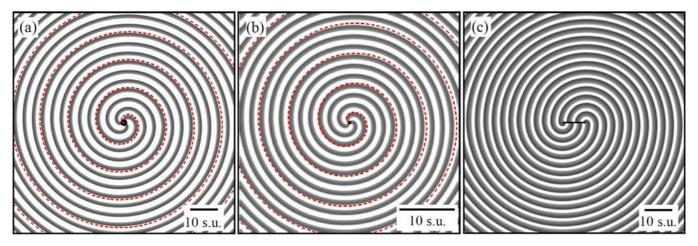


FIG. 6. (Color online) Image overlays of counterclockwise rotating spiral waves pinned to (a) a circle with diameter 5.0 s.u. mm and to rectangles with dimensions (b) 1.3 s.u.  $\times$  1.3 s.u. and (c) 17.0 s.u.  $\times$  0.1 s.u. in the Oregonator model. Dashed curves in (a) and (b) are Archimedean spirals with origins located at the obstacle centers.

the right ends, the wave front near the obstacle has a very high curvature. Then its curvature decreases, while the wave front traces the horizontal upper and lower walls of the obstacle.

In the following, we consider the spiral shapes in Fig. 6(c), as a first attempt to describe the structures of spiral waves pinned to rectangular obstacles. The overlaid image in Fig. 6(c) is separated into two sections: an upper and a lower half as shown in Figs. 7(a) and 7(b), respectively. Interestingly, they look like two halves of the well-known target patterns, which are often observed in excitable media. All wave fronts in both Figs. 7(a) and 7(b) fit to semicircles, the centers of which are close to (but do not touch) the right and the left boundary of the obstacle, respectively. Figures 7(c)-7(e) show a time series of the segment of a wave front close to the obstacle, while the spiral turns around the right boundary. When the segment reaches the lower right corner, it is almost planar and propagates to the right [Fig. 7(c)]. Shortly afterwards it passes the corner and an additional semicircular front appears [Fig. 7(d)]. Subsequently, the semicircular front expands above the obstacle, as if it is emitted from a point source according to the Huygens principle. The center of the point source is located at a distance  $\delta \sim 0.5$  s.u. away from the obstacle wall [Fig. 7(e)]. Note that the distance  $\delta$  is approximately half of the core diameter of a free spiral wave (0.9 s.u.).

Figure 8(a) illustrates a construction of the structure of the spiral wave with its end moving along the upper boundary of a very thin rectangle (dimensions =  $17.0 \text{ s.u.} \times 0.1 \text{ s.u.}$ ) by using the upper and lower semicircles shown in Figs. 7(a) and 7(b). Starting from the wave end attached to the obstacle, the wave front fits to the upper half of the smallest circle C<sub>0</sub>. Then it continues with the lower half of the next circle  $C_1$ . Subsequently, the front alternates to the upper half of the circle  $C_2$  and the lower half of the next circle  $C_3$ , respectively. In Fig. 8(b), centers and radii of the circles are drawn. The centers of C<sub>0</sub> and C<sub>2</sub> are located close to the right boundary of the obstacle, whereas those of  $C_1$  and  $C_3$  are at the left boundary. The centers are far from the boundary at the same distance ( $\delta \sim 0.5$  s.u.). This description is valid for a time interval of about half the rotation period, i.e., during the time that the wave end needs to trace the upper boundary of the obstacle from the right to the left end. Then the wave end turns at the left boundary and a new smallest semicircular wave (new  $C_0$ ) appears at the lower boundary. This spiral shape can

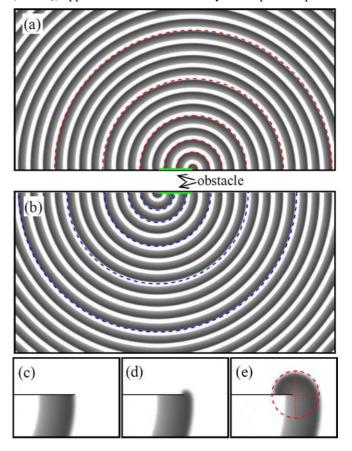


FIG. 7. (Color online) Estimation of the structure of a spiral wave pinned to a very thin rectangle in the Oregonator model. Some wave fronts in (a) the upper and (b) the lower sections of the overlaid image in Fig. 6(c) are compared to semicircles (dashed curves), the centers of which are located close to the right and the left edges of the obstacle. [(c)-(e)] When the wave front turns by an angle of  $180^{\circ}$  at the right boundary, a semicircular front appears, as if it is produced from a point source [the center of the dashed circle in (e)].

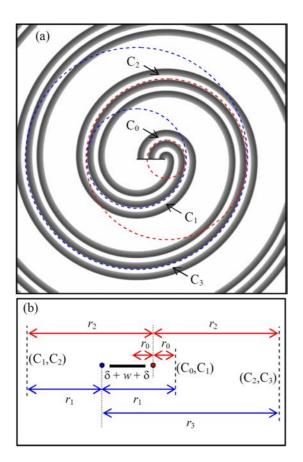


FIG. 8. (Color online) Graphical description of the structure of a spiral wave pinned to a very thin rectangle (black bar) using semicircles. (a) Three consecutive plots of the counterclockwise rotating spiral with the end tracing the upper boundary of the obstacle. The spiral structure at some instant of time can be estimated as a curve that alternately connects upper and lower semicircles of different sizes (corresponding halves of the dashed circles  $C_0$  to  $C_3$ ). (b) Estimation of the radii  $r_0$  to  $r_3$  of the circles  $C_0$  to  $C_3$  having different centers (two small filled circles) close to the left and the right boundary of the obstacle. For the purpose of illustration, the distance  $\delta$  is enlarged to a scale different from that of the width w and the radii  $r_0$  to  $r_3$ . The vertical dashed lines represent the contact positions of semicircle pairs as indicated by the labels.

be described in the same manner after a reorganization of the circles  $C_0$  to  $C_3$  and their centers.

According to the lifetime of the smallest circle  $C_0$ , which is limited to about half of the rotation period as described above, the radius  $r_0$  of the growing  $C_0$  is also limited by the obstacle width w and the distance  $\delta$  of the circle center:  $0 < r_0 \le w + \delta$ . It can be clearly seen in Fig. 8(b) that the radii of the larger circles are related to  $r_0$ , w, and  $\delta$  as  $r_n = r_0 + n(w + 2\delta)$ , where n is an integer.

#### IV. DISCUSSION AND CONCLUSION

We have presented an investigation of spiral waves pinned to unexcitable obstacles with different sizes and shapes in thin layers of the BZ reaction as well as in simulated systems based on the Oregonator model. Circles with increasing areas and circumferences and rectangles with equal areas but different circumferences were chosen as the obstacles. The

results in Figs. 1, 2, 4, and 5 show the common features of the influence of these obstacles on the spiral waves: The pinned spirals propagate with their wavelength, period, and velocity increasing with the obstacle circumference, regardless of the obstacle area. This implies that for such pinning phenomena, the obstacle sizes are more influential due to their circumferences than by their areas.

The time and space units of the simulations are related to the experiments as t.u. =  $1/k_5[MA + BrMA]$  and s.u. =  $\sqrt{D/k_5[MA + BrMA]}$ , where the rate of reaction  $k_5$  and the diffusion D of HBrO<sub>2</sub> are  $0.4 \,\mathrm{M}^{-1}\mathrm{s}^{-1}$  and  $1.5 \times 10^{-5} \mathrm{cm}^2\mathrm{s}^{-1}$ , respectively (cf. Ref. [19]). We used [MA+BrMA] = 0.050 M in the experiments so t.u. = 0.83 min and s.u. = 0.27 mm, which results in the core diameter, wavelength, period, and velocity of the free spiral waves as 0.25 mm, 2.88 mm, 1.29 min, and 2.22 mm min<sup>-1</sup>, respectively. These calculations imply that the excitability in our simulations is relatively higher than that of the real BZ reaction in our experiments, since the simulated spirals had a smaller core diameter, shorter wavelength, shorter period, and higher velocity than for the case of BZ spiral waves. In addition, although our simulations were performed in the excitable regime of the local dynamics [19], we conjecture that pinned spiral waves in oscillatory media would behave in a similar manner. This would hold at least for cases of long period oscillations, because the oscillations will be suppressed by rotating spiral waves with shorter periods, as found in experiments reported earlier [13] as well as in this study.

Tyson and Keener described in Ref. [8] that in determining the angular frequency  $\omega$  and the asymptotic normal velocity c (at locations far from the hole) of a spiral wave rotating around a hole with radius  $r_0$  in a given medium, the curvature relation ( $\omega$  as a function of c and  $r_0$ ) and the dispersion relation (c as a function of  $\omega$ ) must be simultaneously satisfied (see Eq. (24) in Ref. [8]). Both relations are nonlinear and can be solved graphically. Examples for various choices of  $r_0$  in the Oregonator model are given in Fig. 18 of Ref. [8] (a graph of the velocity c versus the period T). It is clear from the intersections of the curves that both the velocity c and the period T of the spiral wave increase simultaneously with the hole radius  $r_0$ . The results also imply that the wavelength  $\lambda$  increases with  $r_0$ , since  $\lambda = c$  T. Thus, our measurements of both circular and rectangular obstacles shown in Figs. 2, 5(b), 5(c), and 5(e) are consistent with the prediction in Ref. [8], even though it was derived only for the circular case. The necessity of the adjustment of the angular frequency  $\omega$  due to the presence of a circular hole in the core region of Archimedean spiral waves has been confirmed in a theoretical study by M. Tsoi [25]. Starting from the curvature effect and the methods employed in Ref. [8], Tanaka et al. [9] showed that the velocity of a spiral wave at the periphery of a circular obstacle increases with the radius of the obstacle (cf. Eq. (8) in Ref. [9]), which agrees well with our results in Figs. 2(d) and 5(d).

Our present findings show that the proposed theories in Refs. [8,9], which predict how the properties of a pinned spiral wave depend on the radius of a circular obstacle, are also valid for other forms (at least for rectangles) after introducing a small modification in the formulas, e.g., replacing the radius r of the circular obstacle by an equivalent quantity  $l/2\pi$  (since  $r = l/2\pi$  for a circle), where l is the obstacle circumference.

Circular obstacles have been used in many investigations of the influence of obstacle size on the release of pinned spiral waves. A train of electrical stimuli with a sufficiently high frequency  $f_{\text{unpin}}$  can induce unpinning of spiral waves. The  $f_{\text{unpin}}$  increases with the obstacle diameter [9,26–28]. An applied electric field causes reorientation and deformation of ring-shaped filaments of three-dimensional spiral waves (so-called scroll rings) that are pinned to a pair of unexcitable spheres in a BZ solution before the filaments are detached from these spheres [29]. A recent investigation [21] on the unpinning of spiral waves by an applied electrical current in the BZ reaction illustrated that a current with a density higher than a critical value  $J_{\text{unpin}}$  can release spiral waves pinned to circular unexcitable objects. Similarly to the frequency  $f_{\text{unpin}}$ , the  $J_{\text{unpin}}$  increases with the obstacle diameter. Further studies on the unpinning of spiral waves from obstacles with other forms, e.g., rectangles, are suggested to elucidate whether the critical value of the forcing (for instance, the frequency  $f_{\text{unpin}}$ of the wave train and the critical current density  $J_{\text{unpin}}$ ) relates solely to the obstacle circumference, as in the case for the properties of pinned spiral waves investigated here.

In contrast to the common features of the parameters of propagation in Figs. 2 and 5, the circular and rectangular obstacles result in different shapes of the spiral waves pinned to them. As shown in Figs. 3 and 6, the spirals are similar to Archimedean ones when pinned to circles or rectangles with a width w similar to the height h ( $w/h \approx 1$ ), while the ones pinned to asymmetric rectangles have unusual forms, which also change with time. The structure of a spiral wave pinned

to a rectangle with extremely high w/h can be described by using semicircles with radii depending on the width w and the core diameter (2 $\delta$ ) of free spirals, as illustrated in Figs. 7 and 8.

It has been shown earlier that the shapes of free spiral waves with circular cores [30] or those pinned to circular obstacles [31] are comparable to Archimedean spirals. Actually, meandering spiral waves rotating about noncircular cores [22 and references therein] have been more often observed, since they occur in broad ranges of system parameters of excitable media. The structures of these spirals, especially for extremely anisotropic cases like Z-shaped and linear cores [32-35], are complicated and have not yet been analyzed sufficiently. We assume that the structure of spiral waves pinned to a very thin rectangular obstacle, as described in this study, is similar to but simpler than that of free spiral waves with linear cores. While the thin rectangle remains at the same location all the time, the orientation of the linear cores is time dependent (see, e.g., Fig. 6(a) in Ref. [32] and Fig. 1(f) in Ref. [34]). Therefore, the fixed thin rectangular obstacle might be taken as a special case of the linear cores that remain stable or change very slowly in time.

#### ACKNOWLEDGMENTS

We thank the Department of Physics, the Faculty of Science, the Research and Development Institute (KURDI), the Center for Advanced Studies of Industrial Technology, the Graduate School, Kasetsart University, and the Thailand Research Fund (Grant No. TRG5680044) for financial support.

- S. Nettesheim, A. von Oertzen, H. H. Rotermund, and G. Ertl, J. Chem. Phys. 98, 9977 (1993).
- [2] F. Siegert and C. J. Weijer, J. Cell Sci 93, 325 (1989).
- [3] J. M. Davidenko, A. M. Pertsov, R. Salomonz, W. Baxter, and J. Jalife, Nature 335, 349 (1992).
- [4] A. T. Winfree, Science 175, 634 (1972).
- [5] J. Ross, S. C. Müller, and C. Vidal, Science 240, 460 (1988).
- [6] A. T. Winfree, Science 266, 1003 (1994).
- [7] E. M. Cherry and F. H. Fenton, New J. Phys. 10, 125016 (2008).
- [8] J. J. Tyson and J. P. Keener, Physica D 32, 327 (1988).
- [9] M. Tanaka, A. Isomura, M. Hörning, H. Kitahata, K. Agladze, and K. Yoshikawa, Chaos 19, 043114 (2009).
- [10] Y. Q. Fu, H. Zhang, Z. Cao, B. Zheng, and G. Hu, Phys. Rev. E 72, 046206 (2005).
- [11] C. Cherubini, S. Filippi, and A. Gizzi, Phys. Rev. E 85, 031915 (2012).
- [12] Z. Y. Lim, B. Maskara, F. Aguel, R. Emokpae, and L. Tung, Circulation 114, 2113 (2006).
- [13] O. Steinbock and S. C. Müller, Physica A 188, 61 (1992).
- [14] K. I. Agladze, R. A. Kocharyan, and V. I. Krinsky, Physica D 49, 1 (1991).
- [15] C. Luengviriya, S. C. Müller, and M. J. B. Hauser, Phys. Rev. E 77, 015201 (2008).
- [16] Z. A. Jiménez, B. Marts and O. Steinbock, Phys. Rev. Lett. 102, 244101 (2009).
- [17] Z. Jiménez and O. Steinbock, Europhys. Lett. **91**, 50002 (2010).

- [18] R. J. Field and R. M. Noyes, J. Chem. Phys. **60**, 1877 (1974).
- [19] W. Jahnke and A. T. Winfree, Int. J. Bif. Chaos 1, 445 (1991).
- [20] C. Luengviriya, U. Storb, M. J. B. Hauser, and S. C. Müller, Phys. Chem. Chem. Phys. 8, 1425 (2006).
- [21] M. Sutthiopad, J. Luengviriya, P. Porjai, B. Tomapatanaget, S. C. Müller, and C. Luengviriya, Phys. Rev. E **89**, 052902 (2014).
- [22] J. Luengviriya, P. Porjai, M. Phantu, M. Sutthiopad, B. Tomapatanaget, S. C. Müller, and C. Luengviriya. Chem. Phys. Lett. 588, 267 (2013).
- [23] M. Dowle, R. M. Mantel, and D. Barkley, Int. J. Bif. Chaos 7, 2529 (1997).
- [24] J. Luengviriya, M. Sutthiopad, M. Phantu, P. Porjai, J. Kanchanawarin, S. C. Müller, and C. Luengviriya. Phys. Rev. E **90**, 052919 (2014).
- [25] M. Tsoi, Persistence of planar spiral waves under domain truncation near the core, Ph.D. thesis, The Ohio State University, 2006.
- [26] K. Agladze, M. W. Kay, V. Krinsky, and N. Sarvazyan, Am. J. Physiol. Heart Circ. Physiol. 293, H503 (2007).
- [27] A. Isomura, M. Hörning, K. Agladze, and K. Yoshikawa, Phys. Rev. E 78, 066216 (2008).
- [28] A. Pumir, S. Sinha, S. Sridhar, M. Argentina, M. Hörning, S. Filippi, C. Cherubini, S. Luther, and V. Krinsky, Phys. Rev. E 81, 010901(R) (2010).
- [29] Z. A. Jiménez, Z. Zhang, and O. Steinbock, Phys. Rev. E 88, 052918 (2013).

- [30] S. C. Müller, Th. Plesser, and B. Hess, Physica D **24**, 87 (1987).
- [31] J. P. Keener and J. J. Tyson, Physica D **21**, 307 (1986).
- [32] V. I. Krinsky, I. R. Efimov, and J. Jalife, Proc. R. Soc. London Ser. A 437, 645 (1992).
- [33] M. A. Dahlem and S. C. Müller, Exp. Brain Res. 115, 319 (1997).
- [34] F. H. Fenton, E. M. Cherry, H. M. Hastings and S. J. Evans, Chaos 12, 852 (2002).
- [35] N. Manz, B. T. Ginn, and O. Steinbock, J. Phys. Chem. A 107, 11008 (2003).